Journal of Applied Physics

TUTORIAL | MARCH 05 2024

Understanding layered compounds under high pressure

J. Pellicer-Porres

J. Appl. Phys. 135, 091101 (2024)
https://doi.org/10.1063/5.0190274

AIP Publishing

Journal of Applied Physics TUTORIAL pubs.aip.org/aip/jap

Understanding layered compounds under high pressure

Cite as: J. Appl. Phys. **135**, 091101 (2024); doi: 10.1063/5.0190274
Submitted: 5 December 2023 · Accepted: 14 February 2024 ·
Published Online: 5 March 2024

J. Pellicer-Porres[a)]

AFFILIATIONS

Departamento de Física Aplicada-ICMUV, Universidad de Valencia, Dr. Moliner 50, Burjassot, 46100 Valencia, Spain

[a)]**Author to whom correspondence should be addressed:** Julio.Pellicer@uv.es

ABSTRACT

This Tutorial focuses on the physics of layered compounds under high pressure. We have chosen h-BN and III–VI layered materials as representative materials. h-BN layers are strictly two-dimensional. Layers in III–VI compounds are more complex, and subtle details in their structural behavior play an important role in the evolution of high pressure properties. They are also interesting because they contain a different number of layers in their primitive unit cell and/or have a different ionic character. We begin describing the structural evolution. We discuss the experimental challenges encountered as well as the main findings related to intra- and interlayer compressibility, polytype influence, and geometrical modifications induced by pressure inside the layers. We then describe lattice vibrations. The origin of the modes is reviewed, paying attention to the relationships between atom motions in different layers. We discuss the convenience of redefining the Grüneisen parameter and describe the behavior of rigid layer modes, soft modes, and Davidov pairs. The last section is devoted to the electronic properties. We show that the changes observed when passing from a single layer to a three-dimensional BN are qualitatively similar to those induced by high pressure. The pressure behavior of electronic transitions in III–VI layered compounds is very rich, revealing the subtle balance between intra- and inter-layer interactions. Finally, we take advantage of high pressure studies to explain the formation of the Mexican hat type of valence band at ambient conditions in single layers of InSe and GaSe, but not in three-dimensional compounds.

I. INTRODUCTION

Pressure is a thermodynamic variable that can induce changes in interatomic spacing that are one or two orders of magnitude larger than those associated with temperature variations, usually without the inherent disorder introduced by temperature. Changes in interatomic spacing lead to changes in the electronic structure and, in extreme cases, challenge basic chemical concepts of bonding. Pressure can be used as a diagnostic tool to test our understanding of matter. This is particularly the case in layered materials, where the relative intensity of intra- and interlayer interactions can be tuned by high pressure.

The mechanical isolation of graphene[1] sparked the interest in 2D materials and van der Waals heterostructures,[2–4] including BN, transition metal dichalcogenides, and layered III–VI chalcogenides, among others. At the same time, the study of two-dimensional materials has renewed the interest in bulk materials. Perhaps, the best example is h-BN. The recent availability of very good quality single crystals[5] has greatly expanded the BN range of applications, not only as an excellent substrate for graphene or as a component in graphene devices but also in photonics.[6] To give just a few examples, even though h-BN is an indirect wide bandgap compound (∼5.9 eV),[7] it exhibits a strong luminescence, which has been used to demonstrate ultraviolet lasing.[8] In addition, its anisotropic structure leads to the formation of hyperbolic phonon polaritons,[9] a key element in nanoscale photonics in the infrared. Its point defects are used as single-photon emitters from the visible to the near-IR range, even at room temperature.[10,11] On the other hand, the initial interest in III–VI layered semiconductors arose because of their applications in the fields of solar cells,[12–15] nonlinear optics,[16–20] and solid-state batteries.[21–24] In this case, however, it is the two-dimensional form that has recently spawned a plethora of applications, as reviewed in Refs. 25 and 26. These include photodetectors, high mobility field effect transistors, and catalytic applications.

Layered materials under high pressure have been studied for decades.[27,28] Recently, several reviews have been published on the high pressure behavior of two- dimensional materials, with a particular focus on summarizing the most relevant recent research[29,30]

and advances in diamond anvil cell (DAC) technology for *in situ* high pressure measurements,[30] or centered in atomically thin van der Waals materials.[31] In this work, we do not pretend to present a review showcasing the most recent research but, instead, describe the behavior of layered compounds under high pressure using a Tutorial approach. We have chosen h-BN and III–VI layered semiconductors as examples, comparing them with graphite where appropriate. Even if they are very relevant from a technological point of view, our choice is based on methodological reasons. h-BN layers are strictly two-dimensional. Layers in III–VI compounds are more complex, and subtle details in their high pressure behavior play a significant role in the evolution of high pressure properties. They are also interesting from a pedagogical point of view because they contain a different number of layers in their primitive unit cell and/or have a different ionic character. We will begin with the evolution of the crystal structures under high pressure (Sec. II). After a brief description of the structural motifs, we discuss the challenges found in high pressure x-ray diffraction experiments on layered materials. We first compare the compressibility of h-BN with that of graphite and then the behavior of β-GaS, ε-GaSe and γ-InSe, including different polytypes. The section concludes reporting x-ray absorption experiments and how they are used to infer the high pressure evolution of the internal intralayer structure. In Sec. III, we discuss lattice vibrations. The origin and physical properties of the modes are described, often relying on symmetry arguments. High pressure studies of the h-BN modes are interesting because, on the one hand, there is a nearly rigid layer mode whose pressure evolution is dictated by the interlayer interaction and, on the other hand, there are two modes with different symmetries, which basically depend on the stretching of the B–N bond but have slightly different pressure evolution. The pressure behavior of lattice vibrations in III–VI layered compounds is exemplified by ε and γ-GaSe. Section IV is devoted to the electronic properties. We first describe the band structure of a BN single layer and then bulk BN, and finally discuss pressure effects with the help of a tight-binding model. The discussion related to III–VI layered semiconductors begins with the description of γ-InSe and then ε-GaSe. The high pressure behavior of optical transitions displays a rich behavior, with the indirect gap decreasing, the direct gap showing a nonlinear dependence on pressure and more energetic direct gaps increasing linearly. All these phenomena can be understood qualitatively in terms of intra- and interlayer interactions. In γ-InSe, the appearance of a toroidal feature in the valence band at high pressure is also described and explained with the help of a $\vec{k} \cdot \vec{p}$ model. Interestingly, a similar feature has been observed in InSe and GaSe single layers.

II. STRUCTURAL PROPERTIES

A. Ambient conditions

We are going to focus our work in the layered materials displayed in Fig. 1. In h-BN, similar to graphene, sp^2 bonding leads to a honeycomb layer where N and B occupy the nonequivalent sites of the hexagons [Fig. 1(a)]. The unit cell includes two layers, stacked in such a way that the B atoms of one layer face N atoms of adjacent layers [Fig. 1(b)]. The resulting structure[32] is centrosymmetric. The inversion center, situated in the interlayer space, relates the two N (or B) atoms of the unit cell.

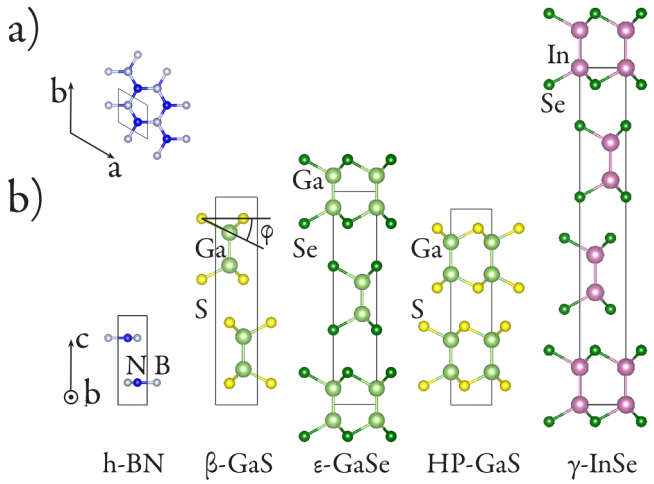

FIG. 1. Sketch of the most relevant structures referred to in this manuscript. (a) [001] view of h-BN. (b) [010] projection of h-BN, β-GaS, and ε-GaSe, the high pressure phase of GaS and γ-InSe. The parallelograms represent the hexagonal unit cell.

Most layered III–VI compounds share the honeycomb layer as structural motif. In this family, however, cations are fourfold coordinated and, as a consequence, the honeycomb is buckled [Fig. 1(b)]. In addition, each layer is doubled, giving rise to a sequence of anion–cation–cation–anion hexagonal planes. The cation–cation distance corresponds to a covalent bond. The stacking of layers results in different polytypes. They can be described using the nomenclature employed in compact structures. We denote by Latin A, B, and C characters the three available positions in an anionic hexagonal layer and with Greek α, β, and γ characters the cationic positions. We begin by considering structures involving two layers. The first layer is symbolized by A$\beta\beta$A. There are several possibilities for the second layer. If we choose B$\alpha\alpha$B, we obtain the β polytype, as in the β-GaS structure.[33] If, instead, we choose the B$\gamma\gamma$B sequence, we form the ε polytype[34] (see ε-GaSe in Fig. 1). The remaining possibility, C$\beta\beta$C, has been found[33] as a high pressure phase of GaS. Let now consider a stacking period of three layers. Even if in principle the possibilities increase, only the so called γ polytype is observed, exemplified here by γ-InSe. The stacking sequence is A$\beta\beta$AB$\gamma\gamma$BC$\alpha\alpha$CA$\beta\beta$A…. In fact, γ-InSe is rhombohedral[35,36] and the primitive unit cell contains only the four atoms defining the layer. Other stacking possibilities involving more layers exist,[34] but we are not going to deal with them in this work. Finally, the *GaTe* structure[37] is more complex, with monoclinic symmetry and one-third of the cation–cation bonds lying nearly parallel to the layers.

Changes in the stacking sequence of the different polytypes imply different elements of symmetry in the resulting structure. In β-GaS and ε-GaSe the environment of each layer is symmetric and there is a mirror plane that relates the two opposed anion–cation planes in a single layer. In β-GaS, anions from one layer face cations from the adjacent layer. As in h-BN, there is an inversion center between the layers that relates atoms from different layers.

There is only one Ga and one S atom in the asymmetric unit, which occupy the 4(f) Wyckoff positions in the $P6_3/mmc$ spatial group. In ε-GaSe, there is no inversion center and the two layers forming the unit cell are not related by symmetry. The asymmetric unit contains one pair of GaSe atoms from one layer and other pair from the adjacent layer. In γ-InSe, the layer environment is not symmetric and there is no mirror plane relating the semi-layers. The asymmetric unit is formed by the two cations and two anions defining a single layer. The rhombohedral primitive unit cell contains only one layer.

The energy difference between polytypes is small, and the structure found experimentally depends on the particular compound and growing method. GaS, the most ionic compound of the III–VI layered family, is only found under ambient conditions as β-GaS. On the opposite, GaSe has not been found in the β polytype.[34,38] Bridgman grown GaSe usually adopts the ε polytype, but it also can be obtained in the γ and δ polytypes.[34] InSe crystals grown by the Bridgman or vapor methods adopt[35,36] the γ polytype, but the crystals are extremely prone to stacking faults, twinning, and the presence of other polytypes in small regions.[36]

h-BN is also very sensitive to stacking faults, which for graphite-like structures are referred to as turbostratic faults. The perfection of the crystalline structure is quantified using a parameter P_3, which is defined as the quotient of layers with the proper

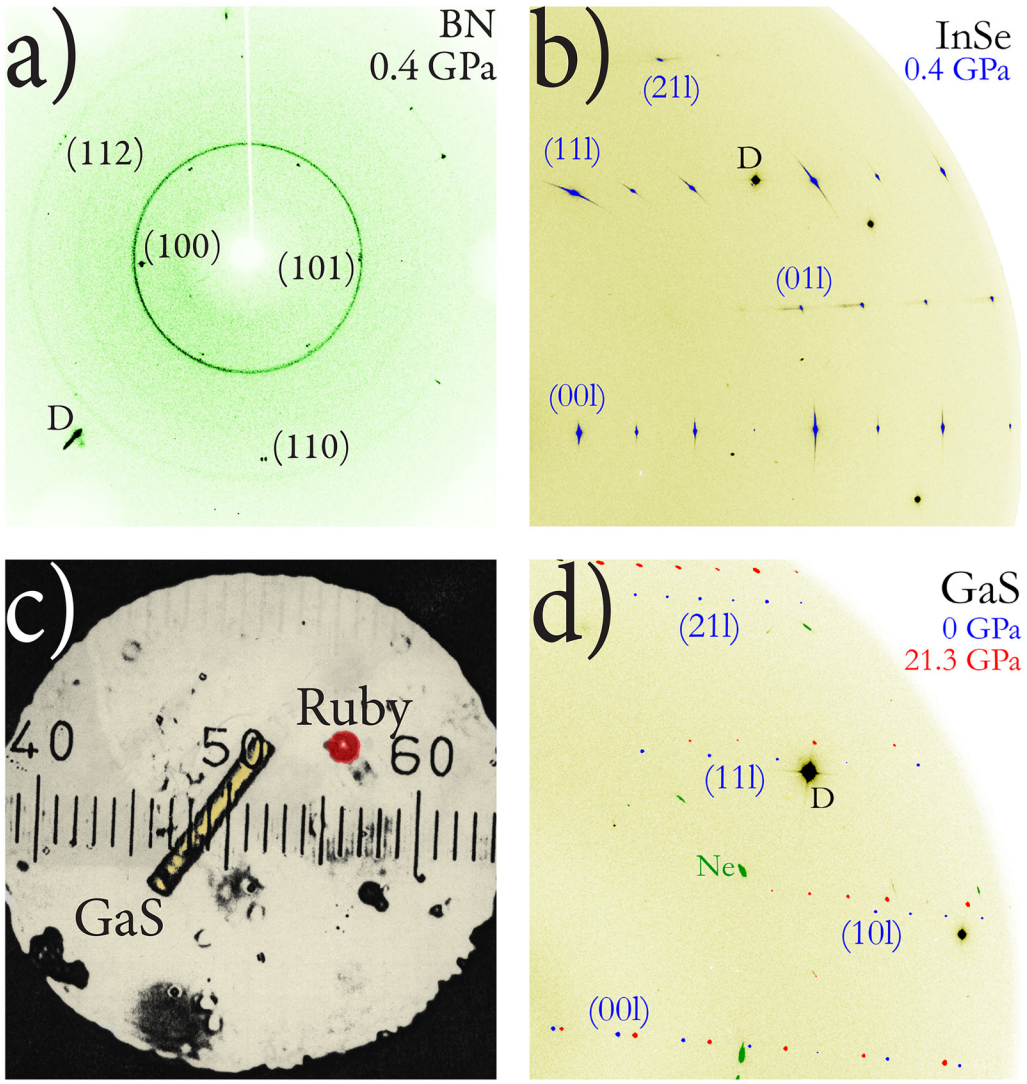

FIG. 2. (a) Image plates from a h-BN single crystal. (110) and (112) reflections evidence a twin. (b) Cutting the γ-InSe single crystal to load the cell results in defect creation and loose in quality of reflections. (c) Photograph of a β-GaS single crystal inside the cell, near the ruby employed to measure pressure. The as grown hexagonal prism had the suitable dimensions to perform the experiment. (d) Digital superposition of two image plates corresponding to the load shown in (c) at two different pressures. The quality of the diffraction spots is maintained. Label D refers to diamond reflections.

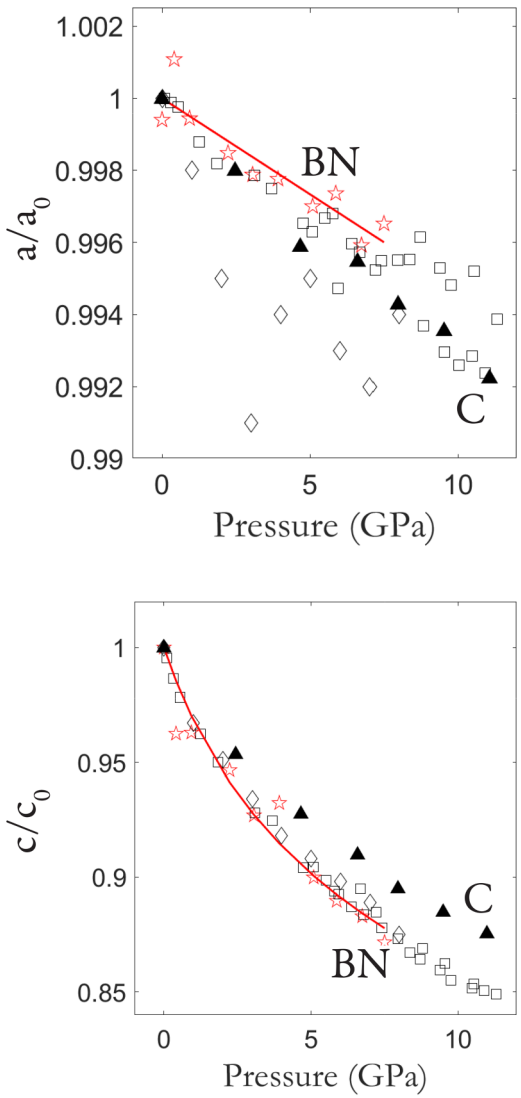

FIG. 3. Lattice parameters of h-BN under high pressure. Red stars correspond to measurements with a single crystal sample, as described in the text. Continuous lines correspond to fits. Hollow squares have been extracted from Ref. 40. Hollow diamonds are reported in Ref. 42. Full symbols correspond to graphite.[47]

arrangement respect to the total number of layers. In h-BN the c lattice parameter has been found to depend on P_3.[39] There is also evidence pointing that as the sample has more defects (P_3 decreases), the finer the powders obtained, the smaller the fragments of the *BN* substructure.

B. High pressure

First, we would like to underline the importance of the sample quality and nature, which in high pressure experiments with layered materials becomes crucial. We begin describing the results found on XRD under pressure in h-BN. Up to very recently, h-BN was prepared only in the powder form. The equation of state found by different authors[40–43] was not consistent (see, for example, Fig. 1 in Ref. 40 or Fig. 1 in Ref. 41). To explain the origin of the discrepancy, emphasis has been given to either turbostratic faults[41] or to stresses and preferred orientation.[44] In Ref. 42, it is underlined the possible response of a layered structure to shear stress and not to hydrostatic pressure. The availability of single crystals[45] induced us to perform high pressure XRD experiments. We employed a diamond anvil cell (DAC) to generate high pressure, a 16:3:1 methanol:ethanol:water (MEW) as pressure transmitting medium and a ruby as a pressure sensor. The single crystal had approximate dimensions of $150 \times 150 \times 30\,\mu m^3$. XRD was performed with a Bruker D8 Advance diffractometer with a Mo anode. We show in Fig. 2(a) the reflections corresponding to the single crystal for a given orientation of the DAC. (110) and (112) reflections evidence a twin, which was probably created when cutting the single crystal with a blade. The detector sample distance was calibrated with CeO_2 powder. The indexation was carried out using ≃50 reflections (6 symmetry independent). Lattice parameters under ambient conditions are a = 2.50(1) Å and c = 6.69(3) Å. Their high pressure evolution is shown in Figs. 3(a) and 3(b) as stars. Note the different scale of both subgraphs. Our data are fully compatible with previous measurements, shown as hollow symbols, in particular, if data for the a axis from Ref. 42 (hollow diamonds) are renormalized. The linear compressibility under ambient conditions is

$$\beta_0 = -\frac{1}{X}\frac{\partial X}{\partial P}\bigg|_0, \tag{1}$$

where X represents a linear length and results in $\beta_0 = 6.5(9)10^{-4}$ GPa^{-1} for the a-axis and $\beta_0 = 3.9(1)10^{-2}$ GPa^{-1} for the c-axis. We compare the compressibility in h-BN with those

TABLE I. Linear compressibility [Eq. (1)] of lattice parameters and bulk modulus in h-BN and related compounds, including cubic BN and carbon related phases. The compressibility is given in GPa^{-1} and the bulk modulus in GPa.

	h-BN	$c-BN$[52]	Graphite[46]	Diamond
β_{a0}	$6.5(9)10^{-4}$	$8.42(4)10^{-4}$	$8.00(6)10^{-4}$	$7.51(2)10^{-4}$, Ref. 53
β_{c0}	$3.9(1)10^{-2}$		$2.8(2)10^{-2}$	
B_0	25.7(7)	396(2)	34(3)	444.5, Ref. 54

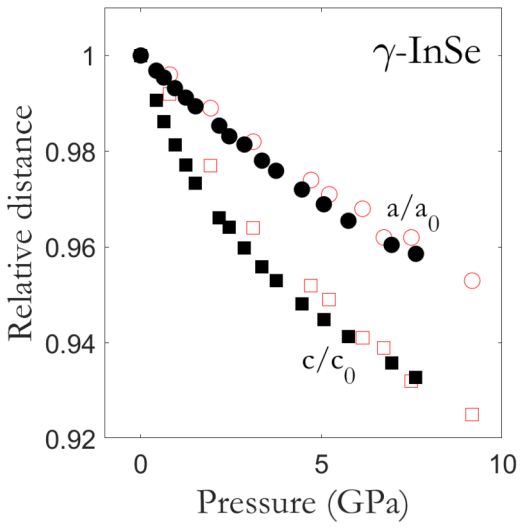

FIG. 4. High pressure evolution of the lattice parameters in γ-InSe. Hollow symbols represent data from an experiment performed with the sample in powder form.[55] Filled symbols correspond to the single crystal employed in Fig. 2(b), as reported in Ref. 56.

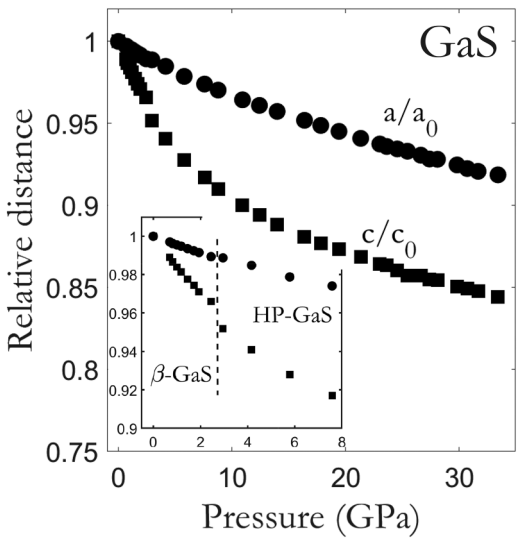

FIG. 5. High pressure evolution of GaS lattice parameters.[56] Data correspond to the experiment of Figs. 2(c) and 2(d). Inset: changes observed near the polytype phase transition taking place at 2.7 ± 0.3 GPa.

of other compounds in Table I. XRD experiments in graphite suffer the same kinds of problems as those explained with h-BN. From the large bibliography available, we have chosen data from Refs. 46 and 47 guided by their mutual agreement and also because the c compressibility matches the one measured with a single crystal.[48] The compressibility of the c-axis in h-BN is two orders of magnitude larger than that of the a-axis, evidencing the stronger covalent bond of the hexagonal layers compared to the van der Waals interaction between layers. The a compressibility is similar to that of cubic BN and also to the a compressibility in graphite. The c-axis compressibility is, however, smaller in graphite than in h-BN (see also Fig. 3). This fact is related to the different stacking patterns in h-BN and graphite. Whereas in h-BN both N and B atoms from different layers face each other,[32] in graphite only half of carbon atoms face atoms of adjacent layers, the other half being above or below the centers of the hexagons.[49] Table I also includes the bulk modulus. It is readily observed that in h-BN and graphite, the bulk modulus is dictated by the intralayer compression ($B_0 \backsimeq 1/\beta_{c0}$).

h-BN and graphite polymorphs are stable up to 10.5 and 14 GPa, respectively.[46,47,50] It is interesting to note that the interlayer distance at the phase transition pressure is the same for both compounds, giving an approximate distance between atoms of adjacent layers of 2.8 Å, which is the same critical distance than the one found in the high pressure amorphization of benzene.[51]

Powder XRD with III–VI layered materials encounters similar problems as those just described in h-BN. In GaSe, powdering seriously affects the ordering.[38] ε-GaSe powder XRD under high pressure is reported in Refs. 57 and 58. Stacking disorder induces the widening of reflections mixing h and k (or l) Miller indexes, in particular, the (103) reflection. InSe is softer than GaSe, and it is even more difficult to prepare a good powder. γ-InSe powder XRD under high pressure has been described in Ref. 55. The evolution of lattice parameters is presented in Fig. 4. We performed XRD under high pressure in γ-InSe single crystals grown by the Brigman method.[56] Cutting the crystal induces irreversible deformations.[36] Figure 2(b) displays the image plate of angle dispersive XRD performed with synchrotron radiation.[56] Even if the diffraction spots become blurred, the quality of the derived equation of state improves with respect to powder XRD, as the comparison performed in Fig. 4 clearly shows. It is interesting to point out that not only the dispersion of the experimental data is reduced when using a single crystal, but also the compressibility of the c-axis near ambient conditions is found to be larger. We only include in Fig. 4 data from the low pressure γ-InSe phase. A phase transition to a rock salt polymorph was found in the powder experiment at 10.3 (5) GPa. In the single crystal experiment, the quality of the spectra diminished from 7.6 ± 0.5 GPa onward, concurrent with the appearance of peaks from the high pressure phase. A variety of techniques have shown the existence of precursor effects at lower pressures, depending on the sensitivity of the technique.[56,59]

The quality of the diffraction data further improves if an as-grown single crystal is used. Figure 2(c) shows a β-GaS single crystal inside the pressure chamber of a diamond anvil cell. The hexagonal needle, prepared by vapor phase transport, had the right dimensions to be used directly in the high pressure experiment. Figure 2(d) is a digital composition displaying simultaneously two image plates measured[56] under ambient conditions (blue reflections) and at 21.3 GPa (red ones). The quality of the reflections is maintained at the largest pressures, with the diffraction spots shifting to the outer positions of the image, i.e., to smaller distances, as pressure increases. The precision of the data allows observing the effect of a polytype phase transition on the cell parameters (Fig. 5). At

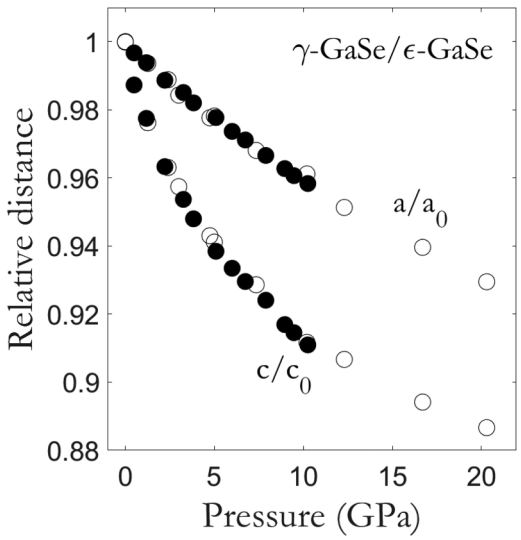

FIG. 6. Comparison between the high pressure evolution of lattice parameters in GaSe for the γ (filled symbols) and ε (hollow symbols) polytypes.

2.7 $\pm$ 0.3 GPa, a sudden decrease (1.5%) in the c parameter is observed. The a axis remains almost constant. The volume decrease in the phase transition is only 0.8%. As described in the structural section, S–Ga–Ga–S layers are unaltered through the phase transition, but the stacking sequence is modified. HP-GaS is stable up to the largest pressure achieved, 35 GPa. This enlarged stability range on the one hand allows demonstrating the nonlinear compressibility of the a axis and, on the other, shows a similar compressibility of both axes is at the largest pressures, when the van der Waals interaction among layers becomes comparable to the intralayer interaction.

We would also like to compare the behavior from two different polytypes of the same semiconductor, γ-GaSe and ε-GaSe. We characterized a vapor phase grown single crystal of γ-GaSe. The experimental conditions of the XRD experiment are those of β-GaS, reported in Ref. 56. The pressure transmitting medium was argon. We compare in Fig. 6 the pressure evolution of the lattice parameters of γ-GaSe with that obtained in the powder experiment described in Ref. 58. We observe that there is no significant discrepancy between both sets of data, apart from the slight increased dispersion of powder data. The compressibility of both polytypes is identical. Recently, state of the art calculations[60] have tried to distinguish between the energy/volume curve of the different polytypes. They have found no difference between the ε and γ polytypes. The most noticeable difference would take place between the ε/γ and β polytypes. This result is interpreted as being related to the interaction of anions and cations from adjacent layers. Whereas in the β polytype, the A$\beta\beta$A B$\alpha\alpha$B stacking sequence involve two pairs of cation–anion interactions, in the ε (A$\beta\beta$A B$\gamma\gamma$B) and γ (A$\beta\beta$A B$\gamma\gamma$B C$\alpha\alpha$C) polytypes, there is only one interaction (see Fig. 1).

We discuss now the compressibility of III–VI layered compounds. Although they are lamellar compounds and, therefore, highly anisotropic, the layers are not strictly two-dimensional as are those of graphite and h-BN. As a result, the compressibility of the a axis of III–VI layered compounds is one order of magnitude larger than that of graphite and h-BN, whereas the compressibility of the c-axis is slightly smaller (compare Tables I and II. Focusing our analysis on Table II, we observe that β_{a0} depends on the cation, being equal in β-GaS γ-GaSe and ε-GaSe and clearly larger in γ-InSe. For its part, β_{c0} does not show any variation between the different compounds under the experimental error, in spite of having the interlayer space defined by S atoms in GaS and larger Se atoms in GaSe. We also do not observe any clear variation in β_{c0} on the polytype.

TABLE II. Linear compressibility [Eq. (1)] of lattice parameters and bulk modulus in III–VI layered compounds. The compressibility is given in GPa^{-1} and the bulk modulus in GPa.

	γ-InSe	β-GaS	γ-GaSe	ε-GaSe
β_{a0}	$70(4)10^{-4}$	$43(3)10^{-4}$	$43(5)10^{-4}$	$43(5)10^{-4}$
β_{c0}	$2.2(1)10^{-2}$	$1.6(4)10^{-2}$	$1.4(2)10^{-2}$	$1.9(5)10^{-2}$
B_0	28(1)	37(4)	44(4)	40(10)

The behavior of β_{a0} in III–VI compounds, both when compared to graphite or h-BN, as well as when considering members of the III–VI family, points to relevant changes in the internal layer arrangement. To access this structural information, it is necessary to measure reliable intensities in a XRD experiment. This is far more difficult than obtaining the lattice parameters. As described above, it is very challenging to obtain a good powder. What is more, the layered character of the compounds inevitably introduces preferential orientations in high pressure experiments. Up to our knowledge, no Rietveld refinement under high pressure has been made. There is only one single crystal XRD experiment, performed in β-GaS up to 6.5 GPa.[33] Another complementary approach based on single crystal x-ray absorption, however, has already been undertaken.[61–64] In this technique, the x-ray energy is chosen close to one absorption edge of a given atom of the sample. X rays ionize the absorbing atom. The spherical wave representing the outgoing electron is backscattered by the atoms surrounding the absorbing atom. The superposition of the outgoing and backscattered wave originates interferences in the post-edge region of the absorption spectrum. From the frequency of the oscillations, it is possible to deduce information about distances between the absorber and backscatterer atoms.[65] We present in Fig. 7 the evolution under high pressure of the cation–anion bondlength in γ-InSe,[61] β-GaS and ε-GaSe.[62] Data from β-GaS have been obtained in the same experiment as the one described in Ref. 62, using a DAC and silicon oil as the pressure transmitting medium. X-ray Absorption Fine Structure (XAFS) was measured at the Ga K-edge. The Extended X-ray Absorption Fine Structure (EXAFS) oscillations were fit using experimental phases and amplitudes extracted from the ambient pressure spectrum. The fit was carried out in the distance space after performing a Fourier transform of the EXAFS signal in the [2.8, 8.2] $Å^{-1}$ wavelength range, using a Bessel ($\tau = 4$) apodization window. The compressibility of the cation–anion bondlength is similar in the three compounds (Table III) and

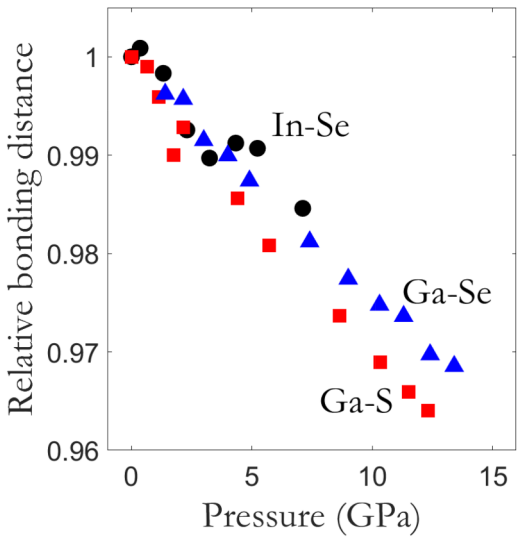

FIG. 7. Evolution of the anion–cation bonding distance under high pressure measured by x-ray absorption in III–VI layered semiconductors.[61,62] The bonding distances have been normalized according to their ambient pressure values.

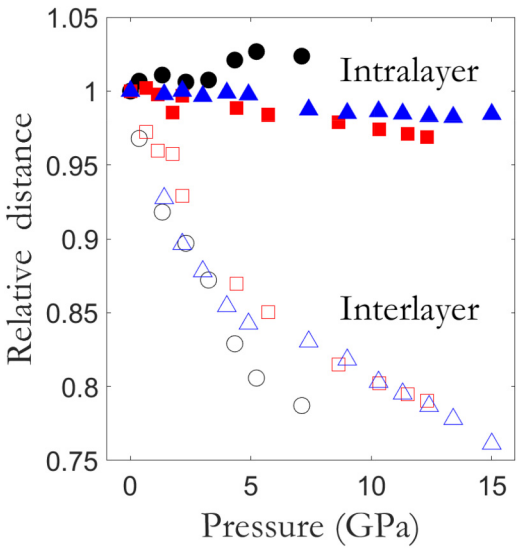

FIG. 8. Evolution of the intra- and interlayer distances under high pressure in III–VI layered semiconductors.[61,62] Data have been normalized according to their ambient pressure values. Squares, triangles, and circles refer to β-GaS, ε-GaSe and γ-InSe respectively.

smaller than that of the a axis. To reconcile β_{a0} and β_{dca0}, the angle φ between the bond and the hexagonal anion planes (Fig. 1) must increase. Geometrically, they are related by

$$\frac{a}{2} = d_{ac}\cos(\varphi)\cos(30). \tag{2}$$

In order to completely describe the high pressure behavior of the layer, we would need the cation–cation bondlength. In the experiments described, the x-ray polarization was perpendicular to the cation–cation bond and then this distance was not accessible. However, in Ref. 33 it was shown than in β-GaS the Ga–Ga and Ga–S compressibility was very similar. Assuming that this behavior can be extrapolated to γ-InSe and ε-GaSe (and extended in pressure in β-GaS), we can calculate the thickness of the intra- and interlayer space along the c axis,

$$\begin{aligned} d_{intra} &= d_{cc} + 2d_{ca}\sin(\varphi), \\ d_{inter} &= \tfrac{c}{n} - d_{intra}, \end{aligned} \tag{3}$$

where d_{cc} and d_{ca} are the cation–cation and cation–anion distances and n is the number of layers in the hexagonal unit cell (n = 3 in γ-InSe and n = 2 in β-GaS and ε-GaSe). The results are presented in Fig. 8 and Table III. We observe a large decrease in the interlayer space, which is of the same order of magnitude as that of the c-axis and approximately the same for the three compounds. The intralayer distance decreases in β-GaS and ε-GaSe, with a compressibility of the same order of magnitude than the a axis, 10^{-3} GPa^{-1}. In γ-InSe, however, the intralayer thickness slightly increases under high pressure. This surprising result has been found in other systems where there is a mixture of covalent as van der Waals interactions, like liquid iodine[66] or crystalline and amorphous selenium.[67,68] In fact, the singularity of γ-InSe is already manifested in having at the same time the largest β_{a0} and the smallest β_{dca0} compressibilities, which necessarily implies the largest φ increment. Notwithstanding that, the evaluation of the intralayer thickness relies on the hypothesis of the cation–cation compressibility. Two *ab initio* calculations reporting[69,70] the detailed structural evolution of γ-InSe under high pressure have been published. Both suggest a more pronounced decrease in the cation–cation distance than in the cation–anion bondlength, and a decrease in the intralayer distance. A definite conclusion can only be given by new experimental data providing access to the cation–cation bondlength.

TABLE III. Linear compressibility [Eq. (1)] of cation–anion bonding distance β_{dca0}, intra- and inter-layer spacing. The compressibility is given in GPa^{-1}.

	γ-InSe[61]	β-GaS	ε-GaSe[62]
β_{dca0}	$2.2(4)10^{-3}$	$3.1(3)10^{-3}$	$2.6(4)10^{-3}$
$\beta_{dintra0}$	$-3.2(6)10^{-3}$	$3.0(3)10^{-3}$	$1.3(2)10^{-3}$
$\beta_{dinter0}$	$34(6)10^{-3}$	$36(9)10^{-3}$	$44(7)10^{-3}$

III. LATTICE VIBRATIONS

We begin this section with h-BN. The primitive unit cell contains four atoms, originating 12 modes. The point group symmetry is 6/mmm. The sixfold axis classifies vibrations according to movements along the hexagonal axis (A or B) or in the layer plane (E). The inversion point, situated between the layers, allows grouping

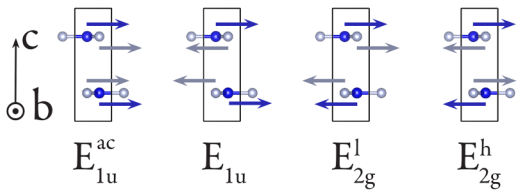

FIG. 9. Phonon patterns of h-BN modes polarized along the layers. Light (gray) arrows represent the movement of B atoms, whereas the movement of nitrogen atoms is represented in a darker (blue) tone.

the modes as odd (subindex u) or even (subindex g). In odd vibrations, the atoms belonging to contiguous layers must vibrate in phase. In even modes, they vibrate in phase opposition.

The in-plane modes are sketched in Fig. 9. The odd mode where the atoms in a layer vibrate in phase is the acoustic mode, E^{ac}_{1u}. If N and B atoms vibrate in phase opposition, they originate an infrared active mode, E_{1u}. With respect to even modes, if N and B atoms vibrate in phase, the phonon pattern is close to a rigid layer mode (the amplitude of B and N may differ), with a low wavenumber given that the added mass of both atoms takes part in the movement and that the interlayer interaction is weak. This is the low E_{2g} mode, labeled E^{l}_{2g}. In the other even mode, where B and N atoms in a layer vibrate in phase opposition, the associated wavenumber is larger. We refer to this mode as the high E_{2g} mode, E^{h}_{2g}. These even modes are Raman active.

The analysis of modes vibrating along the c-axis is analogous. Odd modes include the acoustic and infrared ones, both with A_{2u} symmetry. Even modes, B_{1g}, are silent in this case. The $ABAB\ldots$ stacking sequence, as well as the even character of the modes, makes the polarizability tensor α_{ij} be even with respect to the generalized coordinate Q of the B_{1g} mode, so $\partial\alpha_{ij}/\partial Q\big|_0 = 0$ and the mode is not Raman active.[71] The final decomposition of normal modes in irreducible representations at the Γ point is

$$\Gamma = 2A_{2u} + 2B_{1g} + 2E_{2g} + 2E_{1u}. \tag{4}$$

The wavenumbers corresponding to the optical modes have been compiled in Table IV. The lowest mode is, as expected, the nearly rigid layer mode E^{l}_{2g} [52.6(5) cm^{-1}]. The $B_{1g}(ZA)$ mode [121 cm^{-1}] is also a nearly rigid layer mode, but with a larger restoring force associated with a variation in the interlayer distance, as opposed to the shearing movement of layers in the E^{l}_{2g} mode. The modes with the largest wavenumbers are those involving the stretching of the B–N bond, as in the E^{h}_{2g} and $E_{1u}(TO)$ modes [1368(1) and 1365(3) cm^{-1}, respectively]. Under ambient conditions, the interlayer contribution to the restoring force is negligible, and both modes show similar wavenumbers. If the phonon pattern is along the c-axis, the stretching is not so effective, and the wavenumber decreases to 767(3) cm^{-1} in the $A_{2u}(TO)$ mode and to 810 cm^{-1} in $B_{1g}(ZO)$. It is interesting to note that the $B_{1g}(ZO)$ mode, where B and N atoms of neighbor layers vibrate in phase, has a larger wavenumber than the $A_{2u}(TO)$, where these same atoms vibrate in phase opposition and there is a bonding interaction between B and N which, as we are going to show, plays an important role under high pressure.

TABLE IV. h-BN vibration modes. Wavenumbers are expressed in cm^{-1} and pressure coefficients in cm^{-1}/GPa.

	ω_0	$\partial\omega_0/\partial P\|_0$
E^{l}_{2g} [a]	52.6(5)	8.0(2)
E^{h}_{2g} [a]	1368(1)	4.8(4)
$E_{1u}(TO)$ [b]	1365(3)	3.4(4)
$E_{1u}(LO)$ [b]	1623(3)	4.0(4)
$A_{2u}(TO)$ [b]	767(3)	−8.3(8)
$A_{2u}(LO)$ [b]	825(3)	0.9(1)
$B_{1g}(ZA)$ [c]	121	…
$B_{1g}(ZO)$ [c]	810	…

[a]Exp., Ref. 50.
[b]Exp., Ref. 72.
[c]Theo., Ref. 73.

The high pressure evolution of the modes, as measured by Raman[50] and infrared[72] spectroscopies, is presented in Fig. 10. The behavior of the A_{2u} modes stands out as it is the only mode with a negative pressure coefficient. *Ab initio* calculations under high pressure[74] have shown that modes involving dynamical buckling of the hexagonal layers have negative pressure coefficients. Even if the modes do not destabilize the structure (wavenumbers remain positive), it has been proposed[74] that the interlayer interaction associated with buckling, enhanced by the polar character of the lattice, eases the hexagonal to wurtzite phase transition.

The E^{l}_{2g} mode is the E mode with the largest pressure coefficient. In relative terms, the variation is even more drastic, and it

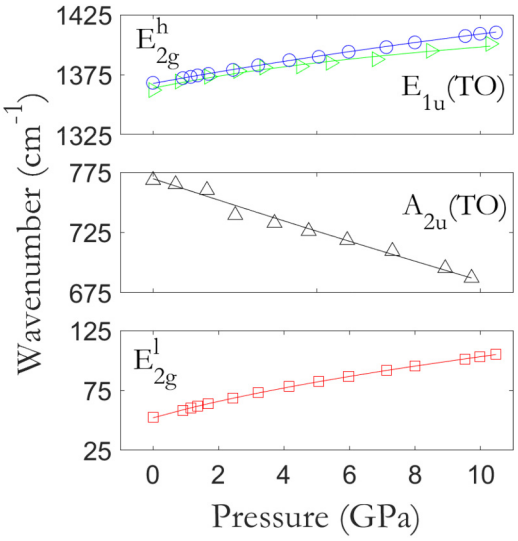

FIG. 10. Pressure evolution of Raman[50] and infrared[72] active modes in h-BN. Lines correspond to fits.

doubles from ambient conditions to 10 GPa. E^h_{2g} and $E_{1u}(TO)$ show similar trends, but careful inspection shows that the frequency separation between both modes increases with pressure.

Application of external pressure to a lattice held together by perfect springs would compress the crystal volume but leave all phonon frequencies unaltered. In the harmonic approximation, force constants do not depend on volume. To describe the dependence of frequency with pressure, it is useful to define a Grüneisen parameter γ,

$$\gamma = -\frac{\partial \ln \omega}{\partial V}, \tag{5}$$

which is equivalent to assume that the frequency is proportional to $V^{-\gamma}$. In layered materials as h-BN, the strong anisotropic behavior suggests to modify the usual definition and follow an analysis based on the pseudo-Grüneisen parameters $\bar{\gamma}$ defined by[46,75]

$$\omega = \omega_0 (X/X_0)^{-3\bar{\gamma}_X}, \tag{6}$$

where X is a lattice parameter, either a or c. Considering this equation, Fig. 11 shows the logarithmic relationship between the wavenumber and the lattice parameter X. We include data[76] from cubic BN for comparison [$\gamma = 1.4(1)$]. The E^l_{2g} modes shows a clear linear behavior if $X \equiv c$ [$\bar{\gamma}_c = 1.3(1)$], and non-linear if $X \equiv a$, in agreement with the rigid layer character of the mode, where the restoring force is determined by the interlayer interaction. The behavior of E^h_{2g} is slightly sub-linear if $X \equiv a$ [$\bar{\gamma}_a = 2.0(1)$] and manifestly nonlinear if $X \equiv c$. In this case, the phonon pattern involves the stretching of the B–N bond along the layer plane, whose length is defined by the a-axis. In the case of the $E_{1u}(TO)$ mode, the sublinearity in the dependence with the a-axis is more pronounced [$\bar{\gamma}_a = 2.2(1)$]. It has to be taken into account that, whereas the opposed B and N atoms from contiguous layers vibrate in phase in E^h_{2g}, they vibrate in phase opposition in $E_{1u}(TO)$. The interlayer interaction associated with the opposed movement of B and N in the phonon pattern of $E_{1u}(TO)$ comes into play at high pressures. As a final conclusion, we observe that when the right scaling parameter is considered, the Grüneisen parameter has values near 1, even in polymorphs as different as h-BN and c-BN.

We focus now in III–VI layered semiconductors. Their layers are not strictly bidimensional, and the description of the vibrations is more involved. We will describe the results obtained in two different polytypes of GaSe. Readers interested in InSe are referred to the bibliography.[78–82] We begin with the simplest polytype, γ-GaSe. Even if γ-GaSe is usually represented using the hexagonal unit cell to easy comparison with other polytypes (as in Fig. 1), its rhombohedral unit cell includes only the four atoms defining a single layer. Taking into account the $3m$ point group symmetry, any vibration at the Γ point can be decomposed as

$$4A_1 + 4E. \tag{7}$$

As in h-BN, A modes vibrate along the c-axis and E modes represent vibrations along the layer plane. All optic modes are both infrared and Raman active.

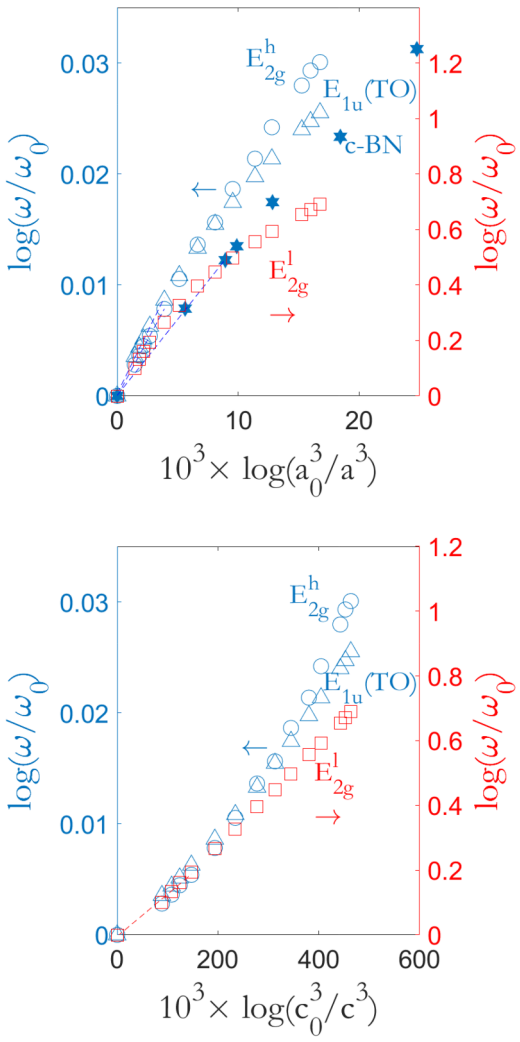

FIG. 11. Analysis of the logarithmic dependence of phonon wavenumbers in h-BN as a function of lattice parameters. For comparison, we include also data from zincblende BN. The scale for the E^h_{2g} (blue circles), $E_{1u}(TO)$ (blue triangles), and zincblende (blue stars) modes is the one on the left (blue). The red right scale is associated with the E^h_{2g} (red squares) phonon. Dashed lines correspond to fits to Eq. (6).

The more common ε-GaSe polytype contains two layers in the unit cell (Fig. 1). There are thus eight atoms in the unit cell, originating 24 normal modes. Point group $\bar{6}m2$ classifies the vibrations at zone center in terms of the following irreducible representations:

$$4A_1' + 4A_2'' + 4E' + 4E''. \tag{8}$$

Modes denoted with a single quote remain invariant when the mirror plane connecting the two hemi-layers is applied. Those modes with double quotes change sign. One A_2'' and one E' mode

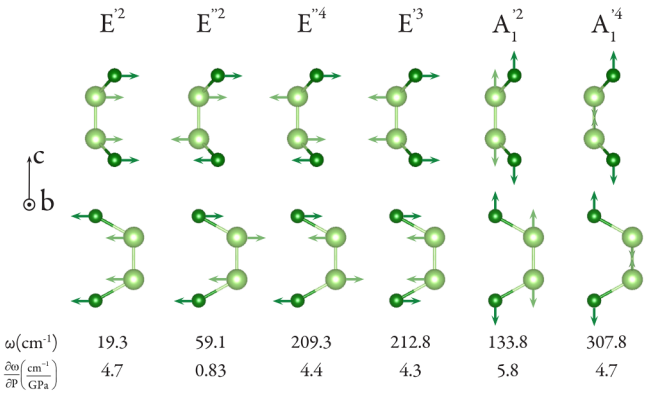

FIG. 12. Phonon patterns of those modes of ε-GaSe, which have been measured under high pressure.[77] We include also the frequencies and pressure coefficients under ambient conditions.

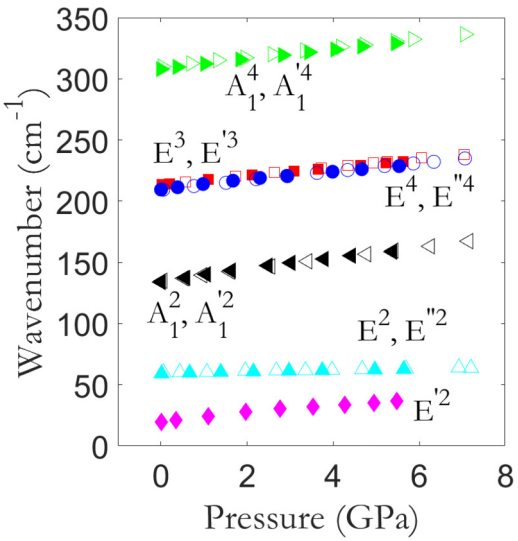

FIG. 13. Pressure dependence of measured[77] Raman active modes in ε-GaSe (full symbols) and γ-GaSe (hollow symbols). The E'^2 mode in ε-GaSe corresponds to the rigid layer mode and has no equivalent in γ-GaSe.

are the acoustic modes. The other three A_2'' vibrations are infrared active only. Modes with A_1', E', and E'' symmetry are Raman active. E' modes are simultaneously Raman and infrared active. In contrast to h-BN, there is no inversion center relating the movement of the two layers as a whole. Their movement is, however, related by translation symmetry. The stacking of two layers doubles the dimensions of the c-axis in ε-GaSe with respect to γ-GaSe, inducing a folding of the Brillouin zone along the (00ξ) direction.[83] The transversal acoustic mode of γ-GaSe at the border zone (special point labeled A) implies a movement in phase opposition of two contiguous layers belonging to two different units cells. The folding in ε-GaSe originates the rigid layer mode E'^2 shown in Fig. 12. Analogous arguments can be applied to optical modes. Given the large difference between intra- and interlayer interactions, their dispersion along ΓA is small[84] and the folding of optical branches in γ-GaSe originates nearly degenerate modes in ε-GaSe, called Davydov pairs. Phonon patterns in Davydov pairs imply either in-phase or out of phase movement of Se atoms defining the interlayer space, so the interlayer electronic density changes very differently in each mode of the pair, implying that their Raman intensity is markedly different. Being close in wavenumber, and with very different intensities, they are very difficult to characterize experimentally.[83,85] High pressure studies[77,86,87] have characterized six Raman active modes: the E'^2 mode originated from the acoustic branch and the most intense components of five Davydov doublets.

Figure 12 represents a sketch of the selected modes in ε-GaSe. Their pressure evolution is shown in Fig. 13 by full symbols, together with the pressure evolution of modes in γ-GaSe (hollow symbols). Red shift of the optical gap precludes obtaining reliable data at pressures larger than 6 GPa.[77] It is clear that modes in γ and ε-GaSe representing the same intralayer movement have the same wavenumbers, even at high pressure. We recall that lattice parameters change in exactly the same way in both polytypes (Fig. 6). It appears that even when the interlayer interaction becomes relevant, the differences in the stacking patters associated with the γ and ε polytypes do not affect the lattice dynamics, except for the symmetry driven apparition in ε-GaSe of the rigid layer mode, E'^2.

The rigid layer mode E'^2 has the smallest wavelength, as expected given the large mass of the layer. It is the only mode where a sublinear dependence with pressure is observed. This fact can be interpreted in terms of its dependence on interlayer interactions, which increase very fast in the first compression stages but then tend to saturate.

The second lowest mode in ε-GaSe is the E''^2 mode. It is the lowest in γ-GaSe where, as described above, the phonon pattern includes only one layer and the irreducible representation is E^2. In this mode, two half-layers vibrate in phase opposition, giving rise to a shearing movement (Fig. 12). Their pressure coefficient is the smallest of all the measurable modes. This fact has been interpreted[77,88] as being the result of compensation between the decrease in the Ga–Ga bond length, which tends to increase the frequency under pressure, and charge transfer from the intramolecular space to the intermolecular region. The analogous mode is observed[88,89] in γ-InSe at 40.3 cm^{-1} and in β-GaS at 74 cm^{-1} with similar pressure coefficients, 0.68 and 0.74 cm^{-1}/GPa, respectively.

All modes, except the E''^2 mode, have pressure coefficients near 5 cm^{-1}/GPa. As the wavelength of the E'^2 is so small, its *relative* pressure variation is the largest one. E''^4 and E'^3 involve the stretching of the Ga–Se bond based on shifts along the layer plane. They have very similar wavenumbers, 209 and 213 cm^{-1}. In the $A_1'^2$ mode, it is the Ga–Ga bond the one that stretches. This mode has a slightly larger pressure coefficient, 5.8 cm^{-1}/GPa, probably due to the fact that both Ga and Se in a half-layer are moving in phase toward the interlayer space. In the $A_1'^4$ mode, both the Ga–Ga and Ga–Se bonds are stretched, and this mode results as the one with the largest wavenumber, 308 cm^{-1}.

A similar pressure behavior of the phonon wavenumbers has been obtained[90] in ε-GaSe thin films (please note the incorrect symmetry assignment,[91] probably based on that of the β polytype).

IV. ELECTRONIC STRUCTURE

The electronic structure of h-BN has been the subject of numerous theoretical[92–102] and experimental studies.[93,97,101–105] We present in blue in Fig. 14(a) the electronic structure of a BN single layer, as calculated in Ref. 98. The orbital character of the bands, derived[92] from symmetry considerations, is stated at high symmetry points of the Brillouin zone with blue labels. The assigned character is in agreement with the calculated density of states presented in Refs. 94 and 98. The eight valence electrons of the B and N atoms forming the unit cell are accommodated in the four lowest bands. The bands with s and p_{xy} orbital character are called σ bands. They are involved in the sp^2 hybridization that originates the hexagonal arrangement. The other band, with p_z orbital character, is named π band due to the π-type overlapping between neighbors. σ (π) bands are even (odd) respect to the symmetry plane coincident with the layer. The existence of the mirror plane avoids the interaction of σ and π bands at general points of the Brillouin zone.

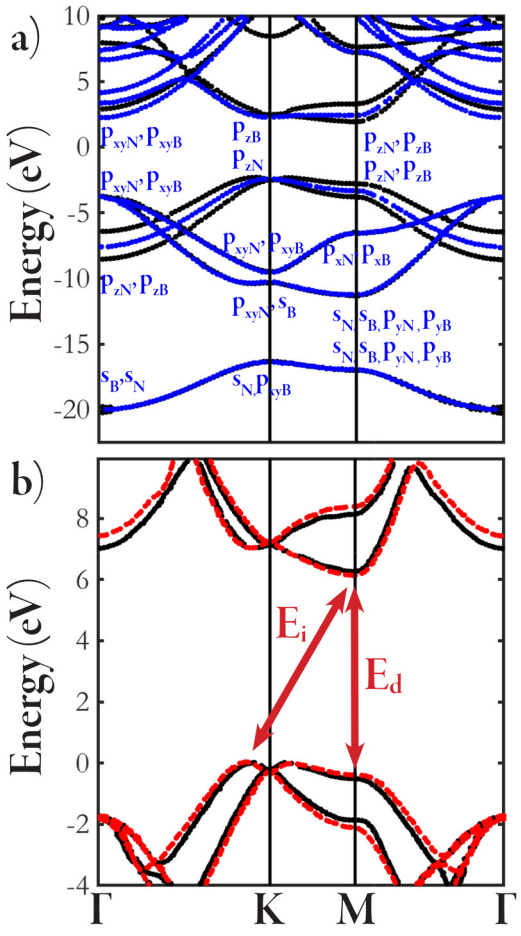

FIG. 14. (a) Ambient pressure electronic structure of a BN single layer (blue points) and bulk h-BN (black points), extracted from Ref. 98. The character of the bands in the case of the 2D compound is assigned in Ref. 92. (b) Bulk h-BN electronic structure under ambient conditions (black points) and at 2.5 GPa, as read from Ref. 106. Please note the usual inconsistency of the bandgap calculated in the two references.

The band structure of the three-dimensional h-BN compound[98] is presented also in Fig. 14(a) as black lines. The unit cell, and, thus, the number of bands, doubles. However, as the overlap between σ orbitals at consecutive layers is not relevant, the new σ orbitals become degenerate. On the opposite, π orbitals split. At Γ, K and M point symmetry avoids interaction between Bloch function derived from p_z orbitals with those derived from s, p_x, and p_y orbitals.[92] At a generic point of the Brillouin zone, the interaction is expected to be small.

Optical properties are dominated by top valence and bottom conduction bands along KM. Their dispersion has been modeled with a tight-binding model[107,108] built on p_{zN} and p_{zB} orbitals. Near K, the valence (conduction) band is dominated by N (B). The conduction band is described by

$$E_{CB} = \Delta + \frac{\left(t_\perp |\gamma(k_\perp)| \pm 2t_\parallel cos(k_\parallel c)\right)^2}{2\Delta}. \quad (9)$$

Here, $\Delta \approx 3.62$ eV is the on site correction to the atomic energy. $t_\perp \approx -2.33$ eV represents the coupling term between first B–N neighbors in the plane and $t_\parallel \approx 0.5$ eV the coupling integral between first B and N atoms facing each other in different layers. Numerical values are obtained fitting the band structure obtained by *ab initio* methods. $k_\perp$ and $k_\parallel$ stand for the wavevector in the plane and perpendicular to it, respectively. $\gamma = \sum_{s=1}^{3} e^{i\vec{k}_\perp \vec{\tau}_s}$ takes into account the phase of wave functions corresponding to the first three neighbors in the plane, described with vector positions $\vec{\tau}_s$.

Let us consider for a moment a single layer of BN ($t_\parallel = 0$). In this model, if only the first neighbor B–N interactions ($t_\perp$) are taking into account, valence and conduction bands would be symmetrical, $E_{VB} = -E_{CB}$. Figure 14, however, shows a flatter conduction band (blue lines). Differences in dispersion are reproduced taking into account the second neighbor N–N and B–B interactions ($t_{2\perp} \approx -0.4$ eV) in the plane (Fig. 4 in Ref. 108).

Experiment and theory agree in assigning a direct bandgap at the K point.[99,104,108] In our model, $\gamma_K = 0$, $|\gamma_M| = 1$ and the conduction band has lower energy at K. Neglecting the second neighbors interactions, the electronic gap at K is approximately given by $2\Delta = 7.24$ eV.[107,108] The optical bandgap is considerably smaller,[104] 6.1 eV, due to huge excitonic effects.[97,105,108]

In the tight-binding model of three-dimensional h-BN the number of p_z orbitals doubles. The splitting is evident in Fig. 14(a), black lines. The physical origin of the splitting is the formation of bonding and antibonding combinations of p_{zN} and p_{zB} orbitals of atoms situated in contiguous layers. This mechanism is not effective at the K point, where $\gamma_K = 0$ and the band has a single energy value, $E_{CB} = \Delta + 2t_\parallel^2/\Delta$. Even if the interlayer interaction is present, the symmetric distribution of first neighbors neutralizes its effect in the LCAO (Linear Combination of Atomic Orbitals) wavefunction for this particular wavevector. At the M point of the Brillouin zone $|\gamma_M| = 1$, and the splitting is maximum, $4t_\parallel t_\perp/\Delta$. In this approximation, the splitting is the same in both valence and

conduction bands. The inclusion of the second neighbor interlayer interactions does not break the degeneracy at the K point but results in a slightly different splitting for both bands at the M point.[108] A global consequence of the splitting is the change of character of the electronic gap, from direct in the monolayer BN to indirect in bilayer and bulk h-BN.[7,97,104] The minimum of the conduction band is at M, whereas the maximum of the valence band is near K.[105,108] The indirect bandgap is around 6 eV.[7,104] The lowest direct gap is now at M.[106]

Figure 14(b) compares the band structure of h-BN under ambient conditions (black) and at 2.5 GPa (red), as calculated in Ref. 106. The pressure evolution of the bands clearly follows the trends observed in the transition from single layer BN to $h-BN$ and can be understood with the aid of the tight-binding model. First of all, the degeneracy at the K point is maintained under high pressure. The direct gap at K, $E_{gd}(K) \approx 2(\Delta + 2t_{\parallel}^2/\Delta)$, increases as a consequence of the augmentation of $t_{\parallel}$ associated with pressure increase. The direct gap at M, $E_{gd}(M) \approx 2\Delta + (t_{\perp} + 2t_{\parallel})^2/\Delta$ decreases due to the larger pressure coefficient of the positive $2t_{\parallel}$ term, which compensates the negative $t_{\perp}$ term more effectively as the pressure increases. From the detailed inset of Fig. 4 in Ref. 106, the pressure coefficients of E_{gd} at M and K can be estimated and then conclude $dt_{\parallel}/dP \approx 40\,\text{meV/GPa}$ and $dt_{\perp}/dP \approx -30\,\text{meV/GPa}$. It should be noticed that not only $t_{\parallel} = 0.5\,\text{eV}$ is significant respect to $t_{\perp} = -2.33\,\text{eV}$ under ambient conditions, but also their pressure coefficients have the same order of magnitude, even if $dt_{\parallel}/dP$ is larger. The analysis of the pressure dependence of the indirect gap requires the description of the maximum of the valence band along ΓK, which is shown in Ref. 108 to critically depend on the second neighbor interaction in the layer ($t_{2\perp}$). For that reason, the increase in the valence band maximum with pressure is rather small and the pressure coefficient of the indirect gap is roughly half of the direct gap at M. The final pressure behavior of the actual optical gap is, as stated above, modified by huge excitonic effects. The direct exciton is formed by transitions around the K (and H) points of the Brillouin zone. As a consequence, in contrast to the large reduction of the direct gap, the direct exciton transition is essentially unaffected by hydrostatic pressure.[106] High pressure enhances the indirect character of $h-BN$.

There have been two experimental high pressure characterizations of the optical gap. Sapphire anvils must be used to generate pressure in order to avoid absorption by the most commonly employed diamond anvils at energies close to the absorption edge. In the first experiment,[109] the absorption coefficient was characterized using a $\sim 20\,\mu$m sample. Given the large absorption coefficient of $h-BN$, only the low energy tail of the absorption edge was characterized. A clear shift to low energies ($-36\,\text{meV/GPa}$) was attributed to the decrease in the direct bandgap. In the second experiment,[106] reflectivity experiments were mainly performed. In this case, two features of the reflectance spectrum were associated with the direct and indirect excitons. Both shift to the red under high pressure, with coefficients $dX_d/dP = -26 \pm 2$ and $dX_i/dP = -36 \pm 2\,\text{meV/GPa}$. After considering the non-trivial excitonic effects, the experimental pressure behavior is in good agreement with the band structure behavior described in the above paragraphs.

Let us now discuss the evolution of the electronic structure of III–VI compounds, beginning with γ-InSe. This compound is a direct semiconductor with an experimentally measured[112] bandgap of 1.27 eV. Figure 15(a) shows a relevant fragment of the γ-InSe band structure as was obtained in the first *ab initio* calculation[110] performed. The direct gap occurs at the Z point of the Brillouin zone. The valence band at this point has a predominant antibonding p_{zSe} character. The conduction band at Z is dominated by antibonding s_{In} orbitals, with some admixture from p_{zSe} antibonding orbitals.[113] The four bands situated below the valence band maximum correspond to $p_{xSe} - p_{ySe}$ bands, grouped in two pairs in the absence of spin–orbit coupling,[110] and 0.3 eV split considering relativistic corrections.[110,113] ΓZ correspond to the direction perpendicular to the layers. The large dispersion of the p_{zSe} band and the extremely low dispersion of $p_{xSe} - p_{ySe}$ bands along this direction evidence that Se p_z orbitals play a fundamental role in

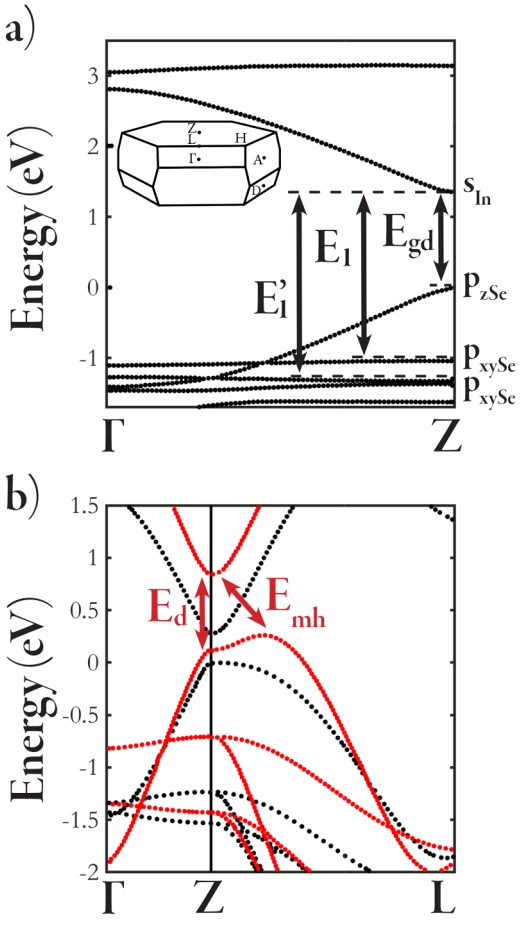

FIG. 15. (a) γ-InSe electronic band dispersion[106,110] along the ΓZ direction, which is perpendicular to the layers. (b) Pressure dependence of the band structure, according to Ref. 111. Black (red) lines display calculations at 0 (7) GPa. Please note the usual inconsistency of the bandgap calculated in the two references.

interlayer interaction, whereas $p_{xSe} - p_{ySe}$ orbitals are basically confined to the layers. The fundamental transition at the Z point is allowed for polarization parallel to the c-axis. It would be forbidden for perpendicular polarization, but the weak hybridization of the p_{zSe} valence band with the underlying $p_{xSe} - p_{ySe}$ bands induced by spin–orbit coupling makes this transition allowed with a small dipole matrix element. Transition from the $p_{xSe} - p_{ySe}$ levels to the conduction band minimum is allowed for polarization perpendicular to the c-axis. The oscillator strength is weak for one of the spin–orbit split pairs.[69,110] The two observed optical transitions are labeled E_1 and E_1'.[113,114] In addition, high pressure studies[115] evidence the existence of an indirect contribution to the absorption edge 0.3 eV above the direct bandgap, which has been assigned to transitions from Γ in the valence band to D in the conduction band[69,115] (not shown in Fig. 15).

ε-GaSe has two layers in the primitive unit cell. Folding the γ-InSe Brillouin zone along ΓZ shifts the direct gap to Γ.[116,117] It is observed experimentally at 2 eV.[77,118,119] The indirect edge[77] is assigned to transitions from Γ to M.[77,116,117] Experimentally, the indirect gap is found to be situated very close to the direct gap.[77,120] β-GaS has a similar band structure than ε-GaSe,[121] with slightly larger dispersion due to stronger orbital hybridization and some more degenerated bands as a consequence of increased symmetry. β-GaS is an indirect semiconductor with a bandgap near 2.5 eV.[122] The indirect gap is proposed to take place at the same points of the BZ than in ε-GaSe. The first direct gap, at Γ, is observed some 0.5 eV above the indirect one.

We include in Fig. 16 the experimental results[113,115,122] concerning the most relevant optical transitions in γ-InSe (in black), ε-GaSe (red), and β-GaS (orange). The direct gap of γ-InSe and ε-GaSe (squares) displays a similar non-linear behavior. At low pressures, the gap decreases, achieves a minimum, and then increases. The minimum is attained at ∼ 0.5 GPa in γ-InSe and at ∼1.2 GPa in ε-GaSe. The indirect gap, also shown in Fig. 16 (circles) displays, opposite to the direct gap, a decreasing nearly linear behavior. The slope increases in modulus in β-GaS respect to ε-GaSe and in ε-GaSe respect to γ-InSe. ε-GaSe and γ-InSe become indirect semiconductors under high pressure.[77,115,123] The same happens in GaTe,[124] another III–VI layered compound not included in this work. The direct transitions E_1 and E_1' present a linear pressure dependence with the same positive slope. The origin and behavior of E_{mh} will be discussed later on.

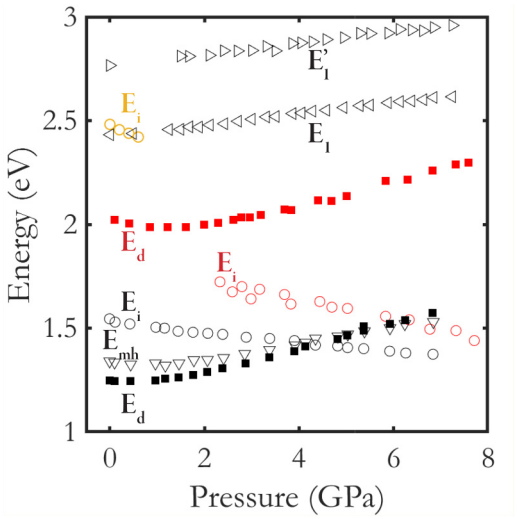

FIG. 16. Pressure evolution of optical transitions as measured[113,115,122] in γ-InSe (in black), ε-GaSe (red), and β-GaS (orange). E_d and E_i stand for the direct (squares) and indirect (circles) gaps. E_1, E_1', and E_{mh} (triangles) are defined in Fig. 15.

The first attempts to describe the high pressure behavior of optical transitions and, in particular, the differences between the decreasing indirect gap and the nonlinear dependence of the direct gap, were based on models of the band structure where, either the position of energy levels,[125] or their splitting,[77,126] was related to intra- and interlayer interactions according to the orbital character of the levels and its contribution to bonding. It became clear[77,126] that all splittings increase with pressure and that deformation potentials corresponding to intralayer interaction are one order of magnitude larger than those of interlayer interactions, as expected from the strength ratio of covalent to van der Waals interactions. The nonlinear shift of a band was assigned[125] to the nonlinearity of the pressure dependence of the van der Waals gap between the layers.

Modern *ab initio* calculations[58,69,113] show the necessity of relaxing the atoms in the layers to their most stable position. They evidence a complex behavior of the layer compression under high pressure, being in agreement with the structural evolution described in Sec. II. They also reproduce the pressure evolution of the gaps and confirm the guidelines just presented. The pressure behavior of the different gaps would be explained as follows below.

Beginning with the direct gap, both the valence band maximum and conduction band minimum shift upward under high pressure. The position of the valence band maximum, whose character is basically p_{zSe}, is affected by the band dispersion in the direction perpendicular to the layers and, thus, by the interlayer interaction. Even if the deformation potential associated with the interlayer interaction is smaller than the intralayer one, the large compressibility of the interlayer space at the initial compression stages induces an initial reduction in the direct gap. At larger pressures, the compressibility is more isotropic and the upward shift of the antibonding metal *s* state related to intralayer compression dominates, causing an increase in the direct gap. It is interesting to note that the evolution under high pressure of the direct gap in InSe has also been studied[81] in near two-dimensional samples with a reduced number of layers. The pressure at which the minimum is observed increases as the number of layers is reduced. This fact has been interpreted[81] on the basis of a progressive increase in the quotient between inter and intralayer deformation potentials, D_{inter}/D_{intra}, as the number of layers is reduced. In samples with a low number of layers ($\lesssim$15), the upward shift of the antibonding metal *s* state associated with intralayer compression is only effective at higher pressures.

E_1 and E_1' are direct transitions with initial (p_{xySe}) and final (metal *s*) states related to antibonding states shifting upward under pressure due to intralayer interaction. Their high pressure behavior is linear, with positive slope. We conclude that the conduction

band has a larger deformation potential. This is reasonable as the bonding contribution of the metal *s* orbitals takes place deep in the valence band (not shown in Fig. 15), whereas the split p_{xySe} bands are located in the upper part of the valence band.

The indirect gap corresponds to transitions between the valence band maximum at Γ and a conduction band minimum situated at the edge of the Brillouin zone (symmetry point M in ε-GaSe and D in γ-InSe). The conduction band minimum shift downward under high pressure and the indirect gap decreases.

In addition to the general qualitative explanation related to intra- and interlayer interactions, the pressure behavior of the bands reveals additional phenomena. Experimentally, an additional indirect gap, E_{mh}, shown in Fig. 16 with downward triangles, is observed in γ-InSe.[111,115] Its pressure dependence is very similar to that of the direct gap. The detailed calculations relate the transition to the formation under high pressure of an upper maximum in the valence band along ZL [Fig. 15(b)] and ZH directions. A detailed analysis of the maximum at pressures larger than 4 GPa reveals that it has quasi-cylindrical symmetry around the c-axis and mirror symmetry with respect to the ZHL plane, giving rise to toroidal constant energy surfaces.[78,127] In ε-GaSe the valence band maximum at Γ flattens under high pressure,[58] but the donut-like feature of the band structure is not developed.[111]

The emergence of the toroidal feature in γ-InSe under high pressure has been explained with the aid of the $\vec{k}\cdot\vec{p}$ model, which describes the curvature of the valence band at the Z point in terms of the following equation for the effective mass m_{vZ}:[111,127]

$$\left[\frac{m_0}{m_{vZ}}\right](k_\perp) = 1 + \frac{2}{m_0}\left(-\frac{|\langle vZ_1|P_\perp|cZ_3\rangle|^2}{E_{cZ3}-E_{vZ1}} + \right.$$
$$+\frac{|\langle vZ_1|P_\perp|cZ_{3A}\rangle|^2}{E_{vZ1}-E_{vZ3A}} + \frac{|\langle vZ_1|P_\perp|cZ_{3B}\rangle|^2}{E_{vZ1}-E_{vZ3B}}$$
$$\left. -\left(A + Bk_\perp^2\right)^2\frac{|\langle vZ_3|P_\perp|cZ_1\rangle|^2}{E_g}\right). \quad (10)$$

The first term in parentheses represents the dipole allowed ($P_\perp$) interaction with p_{xyIn} conduction bands lying 5–6 eV above the valence band maximum. The second and third terms are associated with transitions, also dipole allowed, from the two p_{xySe} valence bands. The first term is negative, and the second and third are positive. If the last term is neglected, the terms in parenthesis nearly cancel, explaining the large effective mass of γ-InSe in the direction perpendicular to the layers, larger than in the parallel direction, resulting in the so-called *anomalous anisotropy*. It is dubbed anomalous because in general, it is expected a large band dispersion along the layers and, thus, a smaller effective mass. The last term is necessary to explain the emergence of the valence band maximum under high pressure. It is related to transitions to the minimum of the conduction band. At exactly the Z point, they would be forbidden by symmetry, but spin–orbit interaction introduces mixing between states from the valence band maximum and underlying p_{xySe} bands. Coefficient A takes into account this effect. The valence band at points other than Z can have a partial p_{xySe} character, originating the $Bk_\perp^2$ term.

A careful analysis of Fig. 16 evidences that the energy difference between the top of the valence band and the p_{xySe} bands decreases in γ-InSe under high pressure.[115] The last term in Eq. (10) eventually dominates under high pressure, compensates the negative terms, and gives rise to a positive curvature of the valence band maximum at Z. The positive curvature is reduced as we get away from Z and $k\perp$ grows, finally becoming negative and leading to the emergence of the maximum in the valence band.

In ε-GaSe, on the opposite, the energy difference between the top of the valence band and the p_{xySe} bands increases as pressure is applied. This fact would explain the nonobservance of the toroidal feature in ε-GaSe under high pressure.[111] The different behavior of the energy difference is, in part, due to the larger compressibility of the In–In bond respect to the Ga–Ga one, which induces a larger splitting of the p_{xySe} bands. It is also due to the weaker intensity of the interlayer interaction, compared to the intralayer one, in γ-InSe respect to ε-GaSe so the shift of the valence band maximum is slower in γ-InSe.

Interestingly, the valence band is also predicted[128–132] to develop a maximum along ΓK in *single layers* of GaS, GaSe and InSe *under ambient conditions*. The resulting band dispersion is usually refereed to as a Mexican hat. The maximum has already been observed in GaSe[133,134] and InSe[135] single layers by angle-resolved photoemission spectroscopy. The model just described is coherent with the calculations performed in InSe and GaSe. In bulk γ-InSe and ε-GaSe $E_{vZ1}-Ev_{Z3A}$ is around 1.0 eV.[58,69,110] At 8 GPa, it is 0.73 eV in γ-InSe.[69] In an InSe single layer under ambient conditions, it is 0.25 and 0.6 eV in a bilayer.[132] Finally, in a GaSe single layer, $E_{vZ1}-E_{vZ3A}$ is ∼0.3 eV.[128] It appears that the observation of the maximum is related to values of $E_{vZ1}-E_{vZ3A}$ clearly below 1 eV. This situation can be achieved either by high pressure in γ-InSe or under ambient conditions by considering the single layer configuration in InSe or GaSe.

V. CONCLUSIONS

We have seen that in order to understand the behavior of layered materials under pressure, it is crucial to previously perform a detailed structural characterization. Given the experimental challenges found with layered materials, it is best to work with single crystals. When layers have an internal structure, like in III–VI semiconductors, x-ray absorption may be very useful in order to determine the layer compressibility and also to characterize geometrical changes inside the layer.

We can extract some general consequences from our description of the structural evolution. The intralayer compressibility under ambient conditions, β_{a0}, is very similar in graphite and in h-BN (Table I), in spite of the different chemical compositions. The interlayer compressibility, β_{c0}, is two orders of magnitude larger than the intralayer one. In III–VI layered compounds, Table II, β_{c0} is of the same order of magnitude than that in graphite and h-BN. We conclude that it is basically determined by the compressibility of the interlayer space, and van der Waals interactions have similar strengths in all the compounds studied. β_{a0} in III–VI compounds is one order of magnitude larger than in graphite and h-BN. The internal structure of the layer can accommodate structural changes as the a lattice parameter is reduced. As a result, β_{c0}

is only one order of magnitude larger than β_{a0}. As the pressure increases, β_a and β_c tend to become more similar, but only in GaS does the large pressure interval of stability of the high pressure phase allow close slopes in the pressure behaviour of a/a_0 and c/c_0 to be observed from about 20 GPa (Fig. 5). The different stacking pattern in graphite and h-BN makes β_{c0} slightly different in both compounds. The influence of the stacking pattern in III–VI compounds is, however, more complex. On the one hand, GaS experiments a first-order phase transition associated with a polytype change (Fig. 5), with a small but measurable volume change. On the other hand, we do not observe any difference in the pressure evolution of γ-GaSe lattice parameters with respect to those of ε-GaSe (Fig. 6). X-ray absorption shows that the pressure evolution of the cation–anion bond length in GaS, GaSe, and InSe is similar to that of the a-axis. Notwithstanding this, a detailed analysis shows that slight variations in the internal geometry of the layers take place under high pressure. The main result is that the intralayer distance hardly decreases under high pressure. New single crystal x-ray diffraction and/or x-ray absorption would be necessary to confirm some of the results, in particular, if the intralayer distance slightly increases in γ-InSe under high pressure.

The section related to lattice vibration includes a detailed discussion of phonon patterns, underlining the relationships between the atoms' movement in different layers and also comparing different polytypes. The rigid layer mode, either the E^l_{2g} mode in h-BN or the E'^2 mode in ε-GaSe, displays the largest relative pressure increase, as the interlayer restoring forces strengthen fast under high pressure. In marked contrast, when the shear movement is associated with opposed hemilayers inside a layer (E''^2 mode in ε-GaSe, Fig. 12, or equivalent modes in InSe and GaS), the pressure coefficient is the smallest one. In h-BN, cations are opposed to anions in contiguous layers. The mode $A_{2u}(TO)$ implies shifts along the c-axis approaching both ions and turns to be a soft mode. In III–VI compounds, the interlayer space is in-between Se atoms, and there is no similar soft mode. Given the simplicity of the h-BN structure, vibrations can be related either to intralayer interactions [E^h_{2g} and $E_{1u}(TO)$] or interlayer ones (E^l_{2g}). Their high pressure behavior is nicely described by a pseudo-Grüneisen parameter related to the appropriate lattice parameter, which happens to have values near 1, as in three-dimensional materials. Davydov pairs in III–VI compounds are very difficult to characterize experimentally, but in h-BN they are readily accessible and distinguishable, as E^h_{2g} is Raman active and $E_{1u}(TO)$ is infrared active. Both are related to B–N stretching and have close wavenumbers under ambient conditions. Interlayer interaction slightly separates them under high pressure. Once again, III–VI layered compounds behave differently at this respect. There is no significant difference between the pressure behavior of equivalent modes in different polytypes (Fig. 13).

The description of the electronic structure begins with BN. We analyze band dispersion with the help of a tight-binding model. We show that the changes observed when passing from single layer to three-dimensional BN are qualitatively similar to those induced by high pressure, Fig. 14. It is remarkable that, in spite of the larger compressibility of the c-axis, the pressure coefficients of the first neighbors coupling integrals in the plane and perpendicular to it, $t_\perp$ and $t_\parallel$, are of the same order of magnitude. The band structure of III–VI layered compounds is also described. The experimental characterization of electronic transitions under high pressure shows a rich behavior, Fig. 16, which can be understood on the basis of the orbital character of initial and final states. The nonlinear pressure dependence of the direct gap is particularly interesting, because it results from a subtle balance between intra- and interlayer interactions. In this case, deformation potentials corresponding to intralayer interaction are one order of magnitude larger than those of interlayer interactions. The balance between intra- and interlayer interactions, as manifested in the direct gap behavior, can be modified either by changing the cation, switching from InSe to GaSe, or by reducing the number of layers in near two-dimensional InSe. Finally, the emergence of the toroidal feature in γ-InSe under high pressure is discussed on the basis of a $\vec{k}\cdot\vec{p}$ model. The formation of such a structure is related to the distance of the upper p_{zSe} valence band to underlying p_{xySe} bands. Interestingly, high pressure helps us to understand the formation of the Mexican hat type of valence band in single layers of InSe and GaSe, but not in three-dimensional compounds under ambient conditions.

ACKNOWLEDGMENTS

I would like to thank financial support from the Spanish Research Agency (AEI) and Spanish Ministry of Science and Investigation (MCIN) under Project No. PID2022-138076NB-C41 and MALTA Consolider Team network, under Project No. RED2022-134388-T. This work was also partially supported by the Generalitat Valenciana under Grant No. PROMETEO CIPROM/2021/075-GREENMAT. This study forms part of the Advanced Materials Programme and was supported by MCIN with funding from European Union NextGenerationEU (PRTR-C17.I1) and by Generalitat Valenciana (Grant No. MFA/2022/007).

AUTHOR DECLARATIONS

Conflict of Interest

The authors have no conflicts to disclose.

Author Contributions

J. Pellicer-Porres: Conceptualization (equal); Data curation (equal); Project administration (equal); Resources (equal); Visualization (equal); Writing – original draft (equal); Writing – review & editing (equal).

DATA AVAILABILITY

Most of the data used in this Tutorial has been already published. Original papers are properly cited. Only one set of XRD data corresponding to BN is new. The data that support the findings of this study are available from the corresponding author upon reasonable request.

REFERENCES

[1]K. S. Novoselov, D. Jiang, F. Schedin, T. J. Booth, V. V. Khotkevich, S. V. Morozov, and A. K. Geim, "Two-dimensional atomic crystals," Proc. Natl. Acad. Sci. U.S.A. **102**, 10451–10453 (2005).

[2]M. Xu, T. Liang, M. Shi, and H. Chen, "Graphene-like two-dimensional materials," Chem. Rev. **113**, 3766–3798 (2013).
[3]A. K. Geim and I. V. Grigorieva, "Van der Waals heterostructures," Nature **499**, 419–425 (2013).
[4]K. S. Novoselov, A. Mishchenko, A. Carvalho, and A. H. Castro Neto, "2D materials and van der Waals heterostructures," Science **353**, aac9439 (2016).
[5]S. Liu, R. He, Z. Ye, X. Du, J. Lin, H. Jiang, B. Liu, and J. H. Edgar, "Large-scale growth of high-quality hexagonal boron nitride crystals at atmospheric pressure from an Fe-Cr flux," Cryst. Growth Des. **17**, 4932–4935 (2017).
[6]J. D. Caldwell, I. Aharonovich, G. Cassabois, J. H. Edgar, B. Gil, and D. N. Basov, "Photonics with hexagonal boron nitride," Nat. Rev. Mater. **4**, 552–567 (2019).
[7]G. Cassabois, P. Valvin, and B. Gil, "Hexagonal boron nitride is an indirect bandgap semiconductor," Nat. Photonics **10**, 262–266 (2016). 1512.02962.
[8]K. Watanabe, T. Taniguchi, and H. Kanda, "Direct-bandgap properties and evidence for ultraviolet lasing of hexagonal boron nitride single crystal," Nat. Mater. **3**, 404–409 (2004).
[9]A. J. Giles, S. Dai, I. Vurgaftman, T. Hoffman, S. Liu, L. Lindsay, C. T. Ellis, N. Assefa, I. Chatzakis, T. L. Reinecke, J. G. Tischler, M. M. Fogler, J. H. Edgar, D. N. Basov, and J. D. Caldwell, "Ultralow-loss polaritons in isotopically pure boron nitride," Nat. Mater. **17**, 134–139 (2018).
[10]R. Bourrellier, S. Meuret, A. Tararan, O. Stéphan, M. Kociak, L. H. Tizei, and A. Zobelli, "Bright UV single photon emission at point defects in *h*-BN," Nano Lett. **16**, 4317–4321 (2016).
[11]T. T. Tran, K. Bray, M. J. Ford, M. Toth, and I. Aharonovich, "Quantum emission from hexagonal boron nitride monolayers," Nat. Nanotechnol. **11**, 37–41 (2016). 1504.06521.
[12]A. Segura, J. P. Guesdon, J. M. Besson, and A. Chevy, "Photoconductivity and photovoltaic effect in indium selenide," J. Appl. Phys. **54**, 876–888 (1983).
[13]J. Martínez-Pastor, A. Segura, J. L. Valdés, and A. Chevy, "Electrical and photovoltaic properties of indium-tin-oxide/p-InSe/Au solar cells," J. Appl. Phys. **62**, 1477–1483 (1987).
[14]C. H. Ho and Y. J. Chu, "Bending photoluminescence and surface photovoltaic effect on multilayer InSe 2D microplate crystals," Adv. Opt. Mater. **3**, 1750–1758 (2015).
[15]M. Teena, A. G. Kunjomana, K. Ramesh, R. Venkatesh, and N. Naresh, "Architecture of monophase InSe thin film structures for solar cell applications," Sol. Energy Mater. Sol. Cells **166**, 190–196 (2017).
[16]R. A. Kaindl, F. Eickemeyer, M. Woerner, and T. Elsaesser, "Broadband phase-matched difference frequency mixing of femtosecond pulses in GaSe: Experiment and theory," Appl. Phys. Lett. **75**, 1060–1062 (1999).
[17]R. S. Putnam and D. G. Lancaster, "Continuous-wave laser spectrometer automatically aligned and continuously tuned from 118 to 161 μm by use of diode-laser-pumped difference-frequency generation in GaSe," Appl. Opt. **38**, 1513 (1999).
[18]F. Keilmann, C. Gohle, and R. Holzwarth, "Time-domain mid-infrared frequency-comb spectrometer," Opt. Lett. **29**, 1542 (2004).
[19]H. Ertap, "Nonlinear absorption, SHG behavior and carrier dynamics of Nd and Pr doped GaSe single crystals," Opt. Mater. **83**, 99–103 (2018).
[20]H. Su, X. Liu, C. Wei, J. Li, Z. Sun, Q. Liu, X. Zhou, J. Deng, H. Yi, Q. Hao, Y. Zhao, S. Wang, L. Huang, S. Wu, W. Zhang, G. Li, and J. Dai, "Pressure-controlled structural symmetry transition in layered InSe," Laser Photonics Rev. **13**, 1900012 (2019).
[21]V. K. Lukyanyuk and Z. D. Kovalyuk, "Sodium intercalation into indium and gallium selenides," Phys. Status Solidi A **102**, K1–K5 (1987).
[22]C. Julien, "Optical studies of the cathode material InSe intercalated with lithium," Solid State Ionics **28-30**, 1167–1171 (1988).
[23]W.-J. Li, Y.-N. Zhou, and Z.-W. Fu, "Fabrication and lithium electrochemistry of InSe thin film," Appl. Surf. Sci. **257**, 2881–2885 (2011).
[24]J. H. Jeong, D. W. Jung, and E. S. Oh, "Lithium storage characteristics of a new promising gallium selenide anodic material," J. Alloys Compd. **613**, 42–45 (2014).
[25]H. Cai, Y. Gu, Y. C. Lin, Y. Yu, D. B. Geohegan, and K. Xiao, "Synthesis and emerging properties of 2D layered III-VI metal chalcogenides," Appl. Phys. Rev. **6**, 041312 (2019).
[26]Z. Yang and J. Hao, "Recent progress in 2D layered III–VI semiconductors and their heterostructures for optoelectronic device applications," Adv. Mater. Technol. **4**, 1–24 (2019).
[27]J. M. Besson, "High-pressure effects in layer semiconductors," Il Nuovo Cimento B Series 11 **38**, 478–485 (1977).
[28]R. Clarke and C. Uher, "High pressure properties of graphite and its intercalation compounds," Adv. Phys. **33**, 469–566 (1984).
[29]L. Zhang, Y. Tang, A. R. Khan, M. M. Hasan, P. Wang, H. Yan, T. Yildirim, J. F. Torres, G. P. Neupane, Y. Zhang, Q. Li, and Y. Lu, "2D materials and heterostructures at extreme pressure," Adv. Sci. **7**, 2002697 (2020).
[30]S. Pei, Z. Wang, and J. Xia, "High pressure studies of 2D materials and heterostructures: A review," Mater. Des. **213**, 110363 (2022).
[31]L. G. Pimenta Martins, R. Comin, M. J. Matos, M. S. Mazzoni, B. R. Neves, and M. Yankowitz, "High-pressure studies of atomically thin van der Waals materials," Appl. Phys. Rev. **10**, 011313 (2023).
[32]R. S. Pease, "An x-ray study of boron nitride," Acta Crystallogr. **5**, 356–361 (1952).
[33]H. D'Amour, W. B. Holzapfel, A. Polian, and A. Chevy, "Crystal structure of a new high pressure polymorph of GaS," Solid State Commun. **44**, 853–855 (1982).
[34]A. Kuhn, A. Chevy, and R. Chevalier, "Crystal structure and interatomic distances in GaSe," Phys. Status Solidi A **31**, 469–475 (1975).
[35]A. Likforman, D. Carré, J. Etienne, and B. Bachet, "Structure cristalline du monosélénure d'indium InSe," Acta Crystallogr. Sect. B **31**, 1252–1254 (1975).
[36]J. Rigoult, A. Rimsky, and A. Kuhn, "Refinement of the 3R indium monoselenide structure type," Acta Crystallogr. **B36**, 916–918 (1980).
[37]M. Julien-Pouzol, S. Jaulmes, M. Guittard, and F. Alapini, "Monotellurure de gallium, GaTe," Acta Crystallogr. Sect. B **35**, 2848–2851 (1979).
[38]J. C. J. M. Terhell and R. M. A. Lieth, "Structures and compounds in the system $Ga_{1-x}Se_x$," Phys. Status Solidi A **10**, 529–535 (1972).
[39]A. V. Kurdyumov, V. L. Solozhenko, and W. B. Zelyavski, "Lattice parameters of boron nitride polymorphous modifications as a function of their crystal-structure perfection," J. Appl. Crystallogr. **28**, 540–545 (1995).
[40]V. L. Solozhenko, G. Will, and F. Elf, "Isothermal compression of hexagonal graphite-like boron nitride up to 12 GPa," Solid State Commun. **96**, 1–3 (1995).
[41]Y. Le Godec, D. Martinez-Garcia, M. Mezouar, G. Syfosse, J. P. Itié, and J. M. Besson, "Thermoelastic behaviour of hexagonal graphite-like boron nitride," High Pressure Res. **17**, 35–46 (2000).
[42]K. Fuchizaki, T. Nakamichi, H. Saitoh, and Y. Katayama, "Equation of state of hexagonal boron nitride," Solid State Commun. **148**, 390–394 (2008).
[43]H. Muhammad, M. Mezouar, G. Garbarino, T. Poreba, G. Confalonieri, M. Ceppatelli, M. Serrano-Ruiz, M. Peruzzini, and F. Datchi, "Anisotropic thermo-mechanical response of layered hexagonal boron nitride and black phosphorus: Application as a simultaneous pressure and temperature sensor," arXiv:2307.07533 [cond-mat.mtrl-sci] (2023).
[44]D. Wakabayashi and N. Funamori, "Solving the problem of inconsistency in the reported equations of state for *h*-BN," High Pressure Res. **35**, 123–129 (2015).
[45]S. Liu, R. He, L. Xue, J. Li, B. Liu, and J. H. Edgar, "Single crystal growth of millimeter-sized monoisotopic hexagonal boron nitride," Chem. Mater. **30**, 6222–6225 (2018).
[46]M. Hanfland, H. Beister, and K. Syassen, "Graphite under pressure: Equation of state and first-order Raman modes," Phys. Rev. B **39**, 12598–12603 (1989).
[47]T. Yagi, W. Utsumi, M. A. Yamakata, T. Kikegawa, and O. Shimomura, "High-pressure in situ x-ray-diffraction study of the phase transformation from graphite to hexagonal diamond at room temperature," Phys. Rev. B **46**, 6031–6039 (1992).
[48]N. Wada, R. Clarke, and S. A. Solin, "X-ray compressibility measurements of the graphite intercalates KC8 and KC24," Solid State Commun. **35**, 675–679 (1980).

[49]P. Trucano and R. Chen, "Structure of graphite by neutron diffraction," Nature **258**, 136–137 (1975).
[50]R. Cuscó, J. Pellicer-Porres, J. H. Edgar, J. Li, A. Segura, and L. Artús, "Pressure dependence of the interlayer and intralayer E_{2g} Raman-active modes of hexagonal BN up to the wurtzite phase transition," Phys. Rev. B **102**, 075206 (2020).
[51]L. Ciabini, M. Santoro, F. A. Gorelli, R. Bini, V. Schettino, and S. Raugei, "Triggering dynamics of the high-pressure benzene amorphization," Nat. Mater. **6**, 39–43 (2007).
[52]F. Datchi, A. Dewaele, Y. Le Godec, and P. Loubeyre, "Equation of state of cubic boron nitride at high pressures and temperatures," Phys. Rev. B **75**, 1–9 (2007). 0702656.
[53]R. Vogelgesang, A. Ramdas, S. Rodriguez, and M. Grimsditch, "Brillouin and Raman scattering in natural and isotopically controlled diamond," Phys. Rev. B **54**, 3989–3999 (1996).
[54]A. Dewaele, F. Datchi, P. Loubeyre, and M. Mezouar, "High pressure-high temperature equations of state of neon and diamond," Phys. Rev. B **77**, 1–9 (2008).
[55]U. Schwarz, A. R. Goñi, K. Syassen, A. Cantarero, and A. Chevy, "Structural and optical properties of InSe under pressure," High Pressure Res. **8**, 396–398 (1992).
[56]J. Pellicer-Porres, E. Machado-Charry, A. Segura, S. Gilliland, E. Canadell, P. Ordejón, A. Polian, P. Munsch, A. Chevy, and N. Guignot, "GaS and InSe equations of state from single crystal diffraction," Phys. Status Solidi B **244**, 169–173 (2007).
[57]M. Takumi, A. Hirata, T. Ueda, Y. Koshio, H. Nishimura, and K. Nagata, "Structural phase transitions of Ga_2Se_3 and GaSe under high pressure," Phys. Status Solidi B **223**, 423–426 (2001).
[58]U. Schwarz, D. Olguin, A. Cantarero, M. Hanfland, and K. Syassen, "Effect of pressure on the structural properties and electronic band structure of GaSe," Phys. Status Solidi B **244**, 244–255 (2007).
[59]F. J. Manjón, D. Errandonea, A. Segura, J. C. Chervin, and V. Muñoz, "Precursor effects of the rhombohedral-to-cubic phase transition in indium selenide," High Pressure Res. **22**, 261–266 (2002).
[60]J. Srour, M. Badawi, F. El Haj Hassan, and A. Postnikov, "Comparative study of structural and electronic properties of GaSe and InSe polytypes," J. Chem. Phys. **149**, 054106 (2018). arXiv:1803.08158.
[61]J. Pellicer-Porres, A. Segura, V. Muñoz, and A. San Miguel, "High-pressure x-ray absorption study of InSe," Phys. Rev. B **60**, 3757–3763 (1999).
[62]J. Pellicer-Porres, A. Segura, C. Ferrer, V. Muñoz, A. San Miguel, A. Polian, J. P. Itié, M. Gauthier, and S. Pascarelli, "High-pressure x-ray-absorption study of GaSe," Phys. Rev. B **65**, 1741031–1741037 (2002).
[63]J. Pellicer-Porres, A. Segura, A. San Miguel, and V. Muñoz, "High pressure EXAFS on GaTe single crystal including polarization," Phys. Status Solidi B **211**, 389–393 (1999).
[64]J. Pellicer-Porres, A. Segura, V. Muñoz, and A. San Miguel, "High-pressure x-ray absorption study of GaTe including polarization," Phys. Rev. B **61**, 125–131 (2000).
[65]D. Konigsberger and R. Prins, *X-ray Absorption: Principles, Applications, Techniques of EXAFS, SEXAFS and XANES* (Wiley Interscience, 1988).
[66]U. Buontempo, A. Filipponi, D. Martínez-García, P. Postorino, M. Mezouar, and J. P. Itié, "Anomalous bond length expansion in liquid iodine at high pressure," Phys. Rev. Lett. **80**, 1912–1915 (1998).
[67]Y. Katayama, H. Kanda, K. Tsuji, O. Shimomura, and H. Oyanagi, "EXAFS study of crystalline selenium under pressure," Physica B **208-209**, 265–266 (1995).
[68]Y. Katayama, K. Tsuji, O. Shimomura, and H. Oyanagi, "EXAFS study of amorphous selenium under pressure," J. Non-Cryst. Solids **205-207**, 199–202 (1996).
[69]D. Olguín, A. Cantarero, C. Ulrich, and K. Syassen, "Effect of pressure on structural properties and energy band gaps of γ-InSe," Phys. Status Solidi B **235**, 456–463 (2003).
[70]K. Z. Rushchanskiĭ, "The influence of hydrostatic pressure on the static and dynamic properties of an InSe crystal: A first-principles study," Phys. Solid State **46**, 179–187 (2004).
[71]P. Brüesch, *Phonons: Theory and Experiment II* (Springer Verlag, 1986).
[72]A. Segura, R. Cuscó, T. Taniguchi, K. Watanabe, G. Cassabois, B. Gil, and L. Artús, "High-pressure softening of the out-of-plane A_{2u} (transverse-optic) mode of hexagonal boron nitride induced by dynamical buckling," J. Phys. Chem. C **123**, 17491–17497 (2019).
[73]J. Serrano, A. Bosak, R. Arenal, M. Krisch, K. Watanabe, T. Taniguchi, H. Kanda, A. Rubio, and L. Wirtz, "Vibrational properties of hexagonal boron nitride: Inelastic x-ray scattering and ab initio calculations," Phys. Rev. Lett. **98**, 12–15 (2007).
[74]G. Kern, G. Kresse, and J. Hafner, "Ab initio calculation of the lattice dynamics and phase diagram of boron nitride," Phys. Rev. B **59**, 8551–8559 (1999).
[75]R. Zallen, "Pressure-Raman effects and vibrational scaling laws in molecular crystals: S_8 and As_2S_3," Phys. Rev. B **9**, 4485–4496 (1974).
[76]S. Ono, K. Mibe, N. Hirao, and Y. Ohishi, "In situ Raman spectroscopy of cubic boron nitride to 90 GPa and 800 K," J. Phys. Chem. Solids **76**, 120–124 (2015).
[77]M. Gauthier, A. Polian, J. M. Besson, and A. Chevy, "Optical properties of gallium selenide under high pressure," Phys. Rev. B **40**, 3837–3854 (1989).
[78]A. Segura, "Layered indium selenide under high pressure: A review," Crystals **8**, 206 (2018).
[79]G. Huang, Y. Zhou, Z. Y. Dong, W. J. Li, K. J. Bu, S. Zhou, T. Wang, X. J. Lü, and X. J. Chen, "Strongly tunable Raman resonance in InSe under pressure," J. Phys. Chem. C **126**, 6344–6350 (2022).
[80]S. Liu, Y. Yang, F. Yu, X. Wen, Z. Gui, K. Peng, R. Wang, and J. Ying, "Pressure-induced superconductivity and nontrivial band topology in compressed γ-InSe," Phys. Rev. B **105**, 214506 (2022).
[81]L. Zhao, Y. Jiang, C. Li, Y. Liang, Z. Wei, X. Wei, and Q. Zhang, "Probing anisotropic deformation and near-infrared emission tuning in thin-layered InSe crystal under high pressure," Nano Lett. **23**, 3493–3500 (2023).
[82]X. Cheng, Z. Huangfu, J. Wang, H. Zhang, S. Feng, Y. Liang, X. Zhu, Z. Wang, X. Wu, and K. Yang, "Structure and anisotropic optical properties of γ-InSe under high pressure," J. Alloys Compd. **970**, 172636 (2024).
[83]A. Polian, K. Kunc, and A. Kuhn, "Low-frequency lattice vibrations of δ-GaSe compared to ε- and γ-polytypes," Solid State Commun. **19**, 1079–1082 (1976).
[84]Z. A. Jahangirli, "First-principles study of the phonon spectrum of ε-GaSe," Phys. Solid State **54**, 1467–1470 (2012).
[85]K. Allakhverdiev, E. Salaev, M. Tagyev, S. Babaev, and L. Genzel, "Davydov doublets in Raman spectra of ε-GaSe," Solid State Commun. **59**, 133–136 (1986).
[86]R. Le Toullec, J. C. Chervin, N. Piccioli, and A. Chevy, "Anharmonic effects in phonon spectra of GaSe," Appl. Opt. **20**, 2566 (1981).
[87]N. Kuroda, O. Ueno, and Y. Nishina, "Lattice-dynamical and photoelastic properties of GaSe under high pressures studied by Raman scattering and electronic susceptibility," Phys. Rev. B **35**, 3860–3870 (1987).
[88]A. Polian, J. C. Chervin, and J. M. Besson, "Phonon modes and stability of GaS up to 200 kilobars," Phys. Rev. B **22**, 3049–3058 (1980).
[89]C. Ulrich, M. A. Mroginski, A. R. Goñi, A. Cantarero, U. Schwarz, V. Muñoz, and K. Syassen, "Vibrational properties of InSe under pressure: Experiment and theory," Phys. Status Solidi B **198**, 121–127 (1996).
[90]N. Q. Diep, S. K. Wu, C. W. Liu, S. H. Huynh, W. C. Chou, C. M. Lin, D. Z. Zhang, and C. H. Ho, "Pressure induced structural phase crossover of a GaSe epilayer grown under screw dislocation driven mode and its phase recovery," Sci. Rep. **11**, 1–10 (2021).
[91]J. Pellicer-Porres, A. Segura, C. Ferrer-Roca, J. González, and V. Muñoz-Sanjose, "Local structure in $Ga_{1-x}In_xSe$ alloys," J. Alloys Compd. **852**, 156365 (2020).
[92]E. Doni and G. P. Parravicini, "Energy bands and optical properties of hexagonal boron nitride and graphite," Il Nuovo Cimento B Ser. 10 **64**, 117–144 (1969).
[93]D. M. Hoffman, G. L. Doll, and P. C. Eklund, "Optical properties of pyrolytic boron nitride in the energy range 0.05–10 eV," Phys. Rev. B **30**, 6051–6056 (1984).
[94]Y. N. Xu and W. Y. Ching, "Calculation of ground-state and optical properties of boron nitrides in the hexagonal, cubic, and wurtzite structures," Phys. Rev. B **44**, 7787–7798 (1991).
[95]J. Furthmüller, J. Hafner, and G. Kresse, "Ab initio calculation of the structural and electronic properties of carbon and boron nitride using ultrasoft pseudopotentials," Phys. Rev. B **50**, 15606–15622 (1994).

[96]X. Blase, A. Rubio, S. G. Louie, and M. L. Cohen, "Quasiparticle band structure of bulk hexagonal boron nitride and related systems," Phys. Rev. B **51**, 6868–6875 (1995).
[97]B. Arnaud, S. Lebègue, P. Rabiller, and M. Alouani, "Huge excitonic effects in layered hexagonal boron nitride," Phys. Rev. Lett. **96**, 1–4 (2006).
[98]M. Topsakal, E. Aktürk, and S. Ciraci, "First-principles study of two- and one-dimensional honeycomb structures of boron nitride," Phys. Rev. B **79**, 1–11 (2009).
[99]J. Kang, L. Zhang, and S. H. Wei, "A unified understanding of the thickness-dependent bandgap transition in hexagonal two-dimensional semiconductors," J. Phys. Chem. Lett. **7**, 597–602 (2016).
[100]R. J. Hunt, B. Monserrat, V. Zólyomi, and N. D. Drummond, "Diffusion quantum Monte Carlo and GW study of the electronic properties of monolayer and bulk hexagonal boron nitride," Phys. Rev. B **101**, 205115 (2020). 2003.06608.
[101]L. Artús, M. Feneberg, C. Attaccalite, J. H. Edgar, J. Li, R. Goldhahn, and R. Cuscó, "Ellipsometry study of hexagonal boron nitride using synchrotron radiation: Transparency window in the far-UVC," Adv. Photonics Res. **2**, 2000101 (2021).
[102]C. Elias, G. Fugallo, P. Valvin, C. L'Henoret, J. Li, J. H. Edgar, F. Sottile, M. Lazzeri, A. Ouerghi, B. Gil, and G. Cassabois, "Flat bands and giant light-matter interaction in hexagonal boron nitride," Phys. Rev. Lett. **127**, 1–6 (2021).
[103]E. Tegeler, N. Kosuch, G. Wiech, and A. Faessler, "On the electronic structure of hexagonal boron nitride," Phys. Status Solidi B **91**, 223–231 (1979).
[104]C. Elias, P. Valvin, T. Pelini, A. Summerfield, C. J. Mellor, T. S. Cheng, L. Eaves, C. T. Foxon, P. H. Beton, S. V. Novikov, B. Gil, and G. Cassabois, "Direct band-gap crossover in epitaxial monolayer boron nitride," Nat. Commun. **10**, 1–7 (2019).
[105]B. Gil, W. Desrat, A. Rousseau, C. Elias, P. Valvin, M. Moret, J. Li, E. Janzen, J. H. Edgar, and G. Cassabois, "Polytypes of sp^2-bonded boron nitride," Crystals **12**, 1–22 (2022).
[106]A. Segura, R. Cuscó, C. Attaccalite, T. Taniguchi, K. Watanabe, and L. Artús, "Tuning the direct and indirect excitonic transitions of *h*-BN by hydrostatic pressure," J. Phys. Chem. C **125**, 12880–12885 (2021).
[107]T. Galvani, F. Paleari, H. P. Miranda, A. Molina-Sánchez, L. Wirtz, S. Latil, H. Amara, and F. Ducastelle, "Excitons in boron nitride single layer," Phys. Rev. B **94**, 1–15 (2016). 1605.09581.
[108]L. Sponza, H. Amara, C. Attaccalite, S. Latil, T. Galvani, F. Paleari, L. Wirtz, and F. Ducastelle, "Direct and indirect excitons in boron nitride polymorphs: A story of atomic configuration and electronic correlation," Phys. Rev. B **98**, 125206-1–125206-17 (2018).
[109]H. Akamaru, A. Onodera, T. Endo, and O. Mishima, "Pressure dependence of the optical-absorption edge of AlN and graphite-type BN," J. Phys. Chem. Solids **63**, 887–894 (2002).
[110]P. Gomes da Costa, R. G. Dandrea, R. F. Wallis, and M. Balkanski, "First-principles study of the electronic structure of γ-InSe and β-InSe," Phys. Rev. B **48**, 14135–14141 (1993).
[111]D. Errandonea, A. Segura, F. J. Manjón, A. Chevy, E. Machado, G. Tobias, P. Ordejón, and E. Canadell, "Crystal symmetry and pressure effects on the valence band structure of γ-InSe and ε-GaSe: Transport measurements and electronic structure calculations," Phys. Rev. B **71**, 1–11 (2005).
[112]J. Camassel, P. Merle, H. Mathieu, and A. Chevy, "Excitonic absorption edge of indium selenide," Phys. Rev. B **17**, 4718–4725 (1978).
[113]C. Ulrich, D. Olguin, A. Cantarero, A. R. Goñi, K. Syassen, and A. Chevy, "Effect of pressure on direct optical transitions of γ-InSe," Phys. Status Solidi B **221**, 777–787 (2000).
[114]N. Kuroda, I. Munakata, and Y. Nishina, "Exciton transitions from spin-orbit split off valence bands in layer compound InSe," Solid State Commun. **33**, 687–691 (1980).
[115]F. J. Manjón, D. Errandonea, A. Segura, V. Muñoz, G. Tobías, P. Ordejón, and E. Canadell, "Experimental and theoretical study of band structure of InSe and $In_{1-x}Ga_xSe$ ($x < 0.2$) under high pressure: Direct to indirect crossovers," Phys. Rev. B **63**, 125330 (2001).
[116]L. Plucinski, L. Johnson, J. Kowalski, K. Kopalko, A. Orlowski, D. Kovalyuk, and V. Lashkarev, "Electronic band structure of GaSe(0001): Angle-resolved photoemission and ab initio theory," Phys. Rev. B **68**, 1–8 (2003).
[117]L. Ghalouci, B. Benbahi, S. Hiadsi, B. Abidri, G. Vergoten, and F. Ghalouci, "First principle investigation into hexagonal and cubic structures of gallium selenide," Comput. Mater. Sci. **67**, 73–82 (2013).
[118]J. M. Besson, K. P. Jain, and A. Kuhn, "Optical absorption edge in GaSe under hydrostatic pressure," Phys. Rev. Lett. **32**, 936–939 (1974).
[119]R. Le Toullec, N. Piccioli, and J. C. Chervin, "Optical properties of the band-edge exciton in GaSe crystals at 10 K," Phys. Rev. B **22**, 6162–6170 (1980).
[120]E. Aulich, J. L. Brebner, and E. Mooser, "Indirect energy gap in GaSe and GaS," Phys. Status Solidi B **31**, 129–131 (1969).
[121]V. N. Brudnyi, S. Y. Sarkisov, and A. V. Kosobutsky, "Electronic properties of GaSe, InSe, GaS and GaTe layered semiconductors: Charge neutrality level and interface barrier heights," Semicond. Sci. Technol. **30**, 115019 (2015).
[122]M. Mejatty, A. Segura, R. L. Toullec, J. M. Besson, A. Chevy, and H. Fair, "Optical absorption edge of gas under hydrostatic pressure," J. Phys. Chem. Solids **39**, 25–28 (1978).
[123]D. Errandonea, F. Manjón, J. Pellicer, A. Segura, and V. Muñoz, "Direct to indirect crossover in III-VI layered compounds and alloys under pressure," Phys. Status Solidi B **211**, 33–38 (1999).
[124]J. Pellicer-Porres, F. Manjón, A. Segura, V. Muñoz, C. Power, and J. Gonzalez, "Optical absorption in GaTe under high pressure," Phys. Rev. B **60**, 8871 (1999).
[125]N. Kuroda, O. Ueno, and Y. Nishina, "Supernonlinear shifts of optical energy gaps in InSe and GaSe under hydrostatic pressure," J. Phys. Soc. Jpn. **55**, 581–589 (1986).
[126]A. R. Goñi, A. Cantarero, U. Schwarz, K. Syassen, and A. Chevy, "Low-temperature exciton absorption in InSe under pressure," Phys. Rev. B **45**, 4221–4226 (1992).
[127]A. Segura, F. Manjón, D. Errandonea, J. Pellicer-Porres, V. Muñoz, G. Tobias, P. Ordejón, E. Canadell, A. San Miguel, and D. Sánchez-Portal, "Specific features of the electronic structure of III-VI layered semiconductors: Recent results on structural and optical measurements under pressure and electronic structure calculations," Phys. Status Solidi B **235**, 267–276 (2003).
[128]V. Zólyomi, N. D. Drummond, and V. I. Fal'Ko, "Band structure and optical transitions in atomic layers of hexagonal gallium chalcogenides," Phys. Rev. B **87**, 195403 (2013).
[129]J. F. Sánchez-Royo, G. Muñoz-Matutano, M. Brotons-Gisbert, J. P. Martínez-Pastor, A. Segura, A. Cantarero, R. Mata, J. Canet-Ferrer, G. Tobias, E. Canadell, J. Marqués-Hueso, and B. D. Gerardot, "Electronic structure, optical properties, and lattice dynamics in atomically thin indium selenide flakes," Nano Res. **7**, 1556–1568 (2014).
[130]V. Zólyomi, N. D. Drummond, and V. I. Fal'Ko, "Electrons and phonons in single layers of hexagonal indium chalcogenides from ab initio calculations," Phys. Rev. B **89**, 205416 (2014).
[131]C. S. Jung, F. Shojaei, K. Park, J. Y. Oh, H. S. Im, D. M. Jang, J. Park, and H. S. Kang, "Red-to-ultraviolet emission tuning of two-dimensional gallium sulfide/selenide," ACS Nano **9**, 9585–9593 (2015).
[132]S. J. Magorrian, V. Zólyomi, and V. I. Fal'Ko, "Electronic and optical properties of two-dimensional InSe from a DFT-parametrized tight-binding model," Phys. Rev. B **94**, 1–20 (2016). 1611.00262.
[133]Z. Ben Aziza, D. Pierucci, H. Henck, M. G. Silly, C. David, M. Yoon, F. Sirotti, K. Xiao, M. Eddrief, J. C. Girard, and A. Ouerghi, "Tunable quasiparticle band gap in few-layer GaSe/graphene van der Waals heterostructures," Phys. Rev. B **96**, 1–8 (2017).
[134]Z. Ben Aziza, V. Zólyomi, H. Henck, D. Pierucci, M. G. Silly, J. Avila, S. J. Magorrian, J. Chaste, C. Chen, M. Yoon, K. Xiao, F. Sirotti, M. C. Asensio, E. Lhuillier, M. Eddrief, V. I. Fal'Ko, and A. Ouerghi, "Valence band inversion and spin-orbit effects in the electronic structure of monolayer GaSe," Phys. Rev. B **98**, 1–7 (2018).
[135]M. J. Hamer, J. Zultak, A. V. Tyurnina, V. Zólyomi, D. Terry, A. Barinov, A. Garner, J. Donoghue, A. P. Rooney, V. Kandyba, A. Giampietri, A. Graham, N. Teutsch, X. Xia, M. Koperski, S. J. Haigh, V. I. Fal'Ko, R. V. Gorbachev, and N. R. Wilson, "Indirect to direct gap crossover in two-dimensional InSe revealed by angle-resolved photoemission spectroscopy," ACS Nano **13**, 2136–2142 (2019).